4-8-2020 11:00 AM

Structure-Function Relationships in the Brain: Applications in Neurosurgery

Daiana-Roxana Pur
The University of Western Ontario

Supervisor
de Ribaupierre, Sandrine
The University of Western Ontario Co-Supervisor
Eagleson, Roy
The University of Western Ontario

Graduate Program in Biomedical Engineering
A thesis submitted in partial fulfillment of the requirements for the degree in Master of Engineering Science
© Daiana-Roxana Pur 2020

Abstract

Multimodal brain imaging allows the study of structure-function relationships of the brain at the individual level, a key subject in basic neuroscience with important applications in neurosurgery. The current thesis aims to better understand these relationships by (1) examining how cortical morphology metrics influence measures of brain function, (2) their visualization in augmented reality (AR), and (3) their application in neurosurgical planning. To achieve these objectives, we made use of multimodal magnetic resonance imaging (MRI) data: diffusion weighted imaging, resting-state functional MRI (rs-fMRI), task-based fMRI, and T1-weighted images. Various metrics were calculated: cortical thickness (CT), blood oxygen level dependent signal variability ($BOLD_{SD}$), structural connectivity (SC), functional connectivity (FC), etc.. We found that $BOLD_{SD}$ measures are confounded by CT, developed an application to visualize SC and FC in AR, and used rs-fMRI to map language for epilepsy surgery. Overall, these studies provided a better understanding of structure-function relationships in the brain.

Keywords

fMRI, neurosurgical planning, neuroimaging, multimodal, brain mapping, resting-state fMRI, augmented reality

Summary for Lay Audience

The human brain is one of the most complex and important organs. Its anatomical structure and its function are inextricably tied to each other in a reciprocal relationship in which structure can shape function and the vice versa. Considering that each person has a unique anatomy, physiology and life experience, it should not come as a surprise that this structure-function relationship is best understood at the individual level. Despite recent advancements in neuroscience, researchers still struggle to understand this relationship and its implications in a clinical setting.

The current thesis aims to explore structure-function relationships of the brain in the setting of basic research and neurosurgery planning. We used multiple distinct but complementary magnetic resonance imaging (MRI) techniques to study these relationships. In the first study, we investigated how cortical morphology metrics (i.e. brain structure measurements) influence a specific measure of brain function called blood oxygen level dependent signal variability ($BOLD_{SD}$) in older adults. $BOLD_{SD}$ has been previously associated with cognitive health in aging. We found that cortical thickness is a confound to $BOLD_{SD}$ measurements and should be considered in the design of studies. In the second study, we examined structure-function relationships by developing an augmented reality application which allows the person using it to explore brain anatomy in the context of brain connectivity (i.e. structural and functional connections between regions in the brain). This application can be further developed to be used as an education tool for novice surgeons. In the third study, we examined the brain scans of children with epilepsy and used structural and functional MRI methods to preoperatively localize language. This can help the surgeon guide their approach to surgery by avoiding brain regions that may be involved in language.

Overall, this thesis adds to the current knowledge of the relationship between the structure and function of brain in the context of basic neuroscience and neurosurgery applications.

Co-Authorship Statement

This thesis consists of three articles, each making up a chapter; the publications listed below are either published or in prepration for publication. All co-authors participated in writing and reviewing the manuscripts. The work was done under the supervision of Sandrine de Ribaupierre and Roy Eagleson.

Chapter 2: **D. R. Pur,** R. A. Eagleson, A. de Ribaupierre, N. Mella, S. de Ribaupierre (2019): *"Moderating Effect of Cortical Thickness on BOLD Signal Variability Age Related Changes"* in Frontiers of Aging Neuroscience, 11. DOI:10.3389/fnagi.2019.00046

My contribution to this chapter included conceiving the research problem, development of the methodology, delineating the steps of the analysis, performing the analysis and the statistics, interpreting the results, generating the figures, and writing the manuscript. Sandrine de Ribaupierre and Roy Eagleson helped conceive and design the steps of the study on the data collected by Nathalie Mella and Anik de Ribaupierre.

Chapter 3: **D. R. Pur,** D. Kikinov, S. de Ribaupierre, R. A. Eagleson (2019): *"Visualization of Mutimodal Brain Connectivity for Neurosurgical Planning using Handheld Device Augmented Reality"* in Proceedings of the 5th World Congress on Electrical Engineering and Computer Systems and Sciences (EECSS'19), 126. DOI: 10.11159/icbes19.126

My contribution included idea development, conceptual design of the application, imaging data pre-processing and analysis, help with participant recruitment for testing, and data collection and analysis. Along, with the other co-authors, I prepared, wrote and reviewed the manuscript. Denis Kikinov contributed by developing and implementing the code for the application, helped with testing, data collection and analysis. Sandrine de Ribaupierre and Roy Eagleson contributed to idea development, and study design.

Chapter 4: D. R. Pur, R. A. Eagleson, S. de Ribaupierre (2020): "*Presurgical brain mapping of the language network in pediatric patients with epilepsy using resting-state fMRI*" in preparation for Journal of Neurosurgery: Pediatrics

My contribution consisted of conception of the study, data collection, study design and methodology development, imaging acquisition, preprocessing and analysis, manuscript preparation, writing and revisions. Sandrine de Ribaupierre was involved in conceiving the project, patient recruitment, imaging acquisition and analysis, and clinical interpretation. Roy Eaglson contributed to idea development and study design and interpretation of the results.

Acknowledgments

I would like to express my heartfelt gratitude to my co-supervisors Dr. Sandrine de Ribaupierre and Dr. Roy Eagleson for their warm guidance, support and mentorship on both a personal and professional level. Thank you for believing in me, it means the world to me. Dr. Eagleson exemplified to me the value of collaboration and collegiality, and offered me valuable advice on different aspects. I immensely admire Dr. de Ribaupierre's professionalism, dedication to her work and family. I am forever grateful for your mentorship.

A special thank you to Dr. Anik de Ribaupierre for sharing her tireless passion for research and life, and for providing me with her invaluable mentorship. I admire her intellectual curiosity, critical spirit and dedication.

In addition, I would like to thank Dr. Ali Khan and Dr. Terry Peters for their feedback, insight, and encouragements during my advisory committee meetings. Your support and reassurance have helped me transition smoothly through the milestones of my graduate degree. I would also like to thank my examiners, Dr. Elvis Chen, Dr. Emma Duerden, and Dr. Jody Culham for taking the time to read my thesis and provide helpful comments.

To the current and past members of the Brain3DViz lab thank you for your support and smiles at the lab meetings. I would like to particularly thank Marcus Lo and Daamoon Ghahari for their endless encouragement and advice.

I am grateful to my friends and family. I especially thank my grandparents for their unconditional love and encouragements throughout my life.

Last but not least, thank you to my partner and best friend Alexsi. I am proud of you. Thank you for your love, patience, advice and for welcoming me into your family.

Table of Contents

List of Tables

List of Figures

List of Appendices

Acronyms

3D	Three-Dimensional
BOLD	Blood-Oxygen-Level Dependent (contrast imaging)
$BOLD_{SD}$	BOLD signal variability
CA	Cortical Area
CT	Cortical Thickness
CSF	Cerebro-spinal Fluid
DTI	Diffusion Tensor Imaging
DWI	Diffusion Weighted Imaging
FC	Functional Connectivity
fMRI	Functional Magnetic Resonance Imaging
GM	Grey Matter
MNI	Montreal Neurological Institute
rs-fMRI	Resting-state fMRI
SC	Structural Connectivity
WM	White Matter

Chapter 1

1   Introduction

1.1   Background and Clinical Motivation

Function within the brain has traditionally been represented in terms of fixed anatomical location. For example, the most popular approach to localizing expressive language within the brain has been to focus on identifying Broca's area (i.e. left inferior frontal cortex) because damage to this area results in specific expressive language deficit or aphasia[1]. With time, it became recognized that representation of language is best understood in terms of networks distributed over various brain regions rather than specific focality[2]. In the 1970's, Whitaker and Selnes[3] discussed the ideas that (1) individual differences in anatomic variations must be considered when localizing function, and that (2) function is not fixed but rather can become reorganized in various conditions (e.g. right hemisphere can take over some speech functions in case of injury to the left hemisphere)[2,3]. These ideas were particularly evident for language because it is a higher order cognitive ability and presents with higher inter-individual variability than motor or sensory functions. With advancements in imaging techniques (i.e. magnetic resonance imaging, MRI), it became increasingly recognized that relationships between the brain structure (i.e. cortical morphology) and function change across lifespan, and the degree of these changes vary by brain regions and from one individual to another[4]. This suggests aging as an interesting setting to better understand structure-function relationships in the brain.

A significant amount of the early knowledge on brain structure-function relationships at the individual level came from lesions and neurosurgical interventions (i.e. resections or stimulation). Cortical stimulation to map eloquent cortex (i.e. areas of the brain that if damaged will lead to severe deficits), described by Penfield in the early 1950's, allowed for investigation of function by linking intra-operative stimulation of neural activity with direct behavioral changes (i.e. speech arrest)[5]. Cortical stimulation remains the gold standard for localizing function in the setting of neurosurgical interventions for conditions such as intractable epilepsy, which require brain mapping of eloquent cortex

surrounding the epileptogenic zone to be resected in order to minimize post-operative deficit. Language mapping in pediatric epilepsy is particularly important because young children are more likely to reorganize function at the intra- and inter-hemispherical level than adults with epilepsy or healthy children[6]. Therefore, in this setting, structure-function relationships can be atypical, and localization of function based on anatomical landmarks alone is usually unreliable. For precise localization, in most cases, stimulation is done at the bedside using subdural or depth electrodes in the setting of staged surgery rather than intraoperatively. However, stimulation studies remain technically challenging in children due to limited compliance and their unique developmental neurophysiology (i.e. cortical immaturity), and so complementary functional MRI (fMRI) based mapping is also obtained when possible [6,7]. Pediatric epilepsy provides an interesting framework to examine structure-function relationships of the brain.

1.2   Fundamentals of Neuroimaging

Magnetic Resonance Imaging (MRI) is a non-invasive imaging tool that utilizes non-ionizing radiation from hydrogen protons in the human body to visualize the brain and any other part of the body. It relies on a very strong main magnetic field, rapidly changing magnetic fields, radio frequency pulses, and a computer to produce cross-sectional images[8]. Cross-sectional imaging allows viewing of images in the form of a plane (e.g. axial) through the body with the structure of interest cut across. Individual images, referred to as slices, are parallel to one of three imaging planes (axial, sagittal, and coronal, Figure 1-1). Images have depth due to slice thickness. Two-dimensional (2D) slices can be stacked (i.e. 2D multi-slice volumes) to create a three-dimensional (3D) representation.

MRI is often divided into structural and fMRI; with structural MRI usually representing static anatomical information and fMRI indicating metabolic fluctuations in function captured over the time of the scan.

1.2.1 Structural MRI

Neuroimaging using structural MRI based on T1-weighted images refers to volumetric, high resolution images of brain structures with high contrast between white (WM) and grey matter (GM) (Figure 1-1).
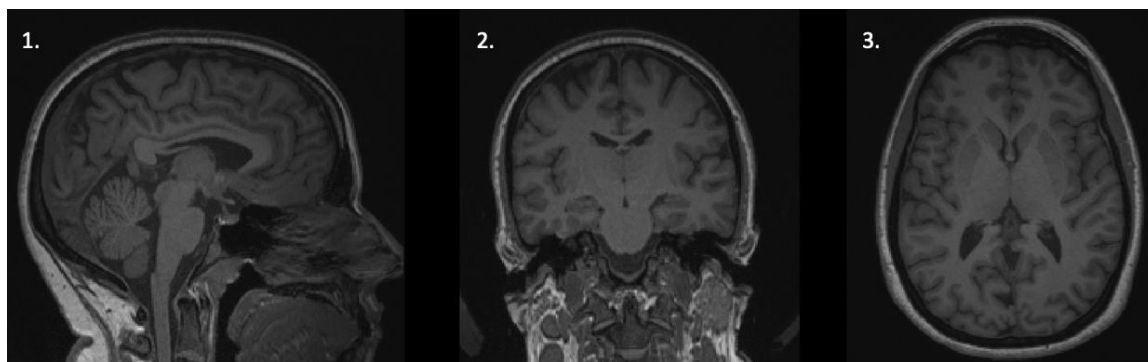
Figure 1-1. T1-weighted structural imaging. Different views are presented: 1) sagittal, 2) coronal, 3) axial. WM is bright, GM is darker.

By using T1-weighted images as input to brain imaging processing and analysis tools (i.e. FreesSurfer[1]), various measurements and representations of the human cortex can be produced. These can vary depending on the software tools used but the pre-processing, processing, and analysis steps are relatively similar across the software packages (see Figure 1-2 for example of use of software tool).

---

[1] https://surfer.nmr.mgh.harvard.edu/
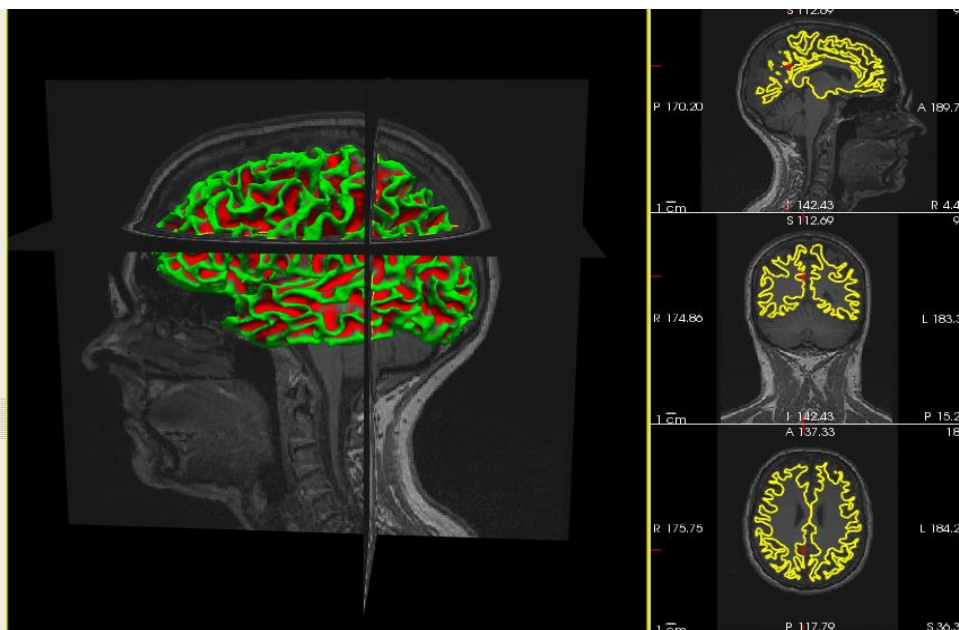
Figure 1-2. T1-weighted image with WM surface model. Software used is FreeSurfer.

 In the methodology section of each study included in the thesis there is a description of the software tools used. In brief, some of the first steps in the preprocessing/analysis pipeline are to register the images to a standard coordinate space or template (i.e. Montreal Neurological Institute, MNI space[9,10]) using linear and/or non-linear matrix transformations, "spatial normalization", and to remove non-brain tissues, "skull stripping". This allows findings from different imaging modalities to be combined and compared. Another common step is to segment the brain into WM , GM and cerebral spinal fluid (CSF): subcortical segmentation and cortical segmentation. Using various algorithms and taking into account the differing intensity of the voxels in these tissues, cortical surface models of the boundaries between cortical GM, WM, and pial surface are produced. These allow automatic estimation of cortical thickness (CT), cortical volume, cortical area, gyrification, curvature, etc.. (described in detail in [11,12]). An atlas is a volumetric or surface based brain map, where each voxel is labelled as being part of specific brain region depending on the map used (also referred to as "parcellation scheme", see review [13]). By using an atlas to parcellate the cortex, region specific measurements of cortical morphology can be determined.

Clinically, T1-weighted images can be used to detect various tissue deformations (i.e. cortical dysplasia), tumors, and to register other imaging modalities with lower resolution or contrast.

1.2.2 Diffusion- weighted MRI

Diffusion-weighted imaging, is an MRI technique based on tissue water diffusion rate (i.e. thermal Brownian motion of water molecules). It can offer information about brain WM architecture and WM integrity in the context of basic neuroscience or clinical applications in neurosurgery (see extensive review[14]). Clinical applications include its use in presurgical planning as it can map major WM tracts.

Basic pre-processing steps are applied to correct for motion, and for image distortions caused by currents generated by rapidly changing gradient magnetic fields (i.e. eddy currents). In brief, at the preprocessing stage the diffusion tensor model (i.e. using a tensor ellipsoid giving the name diffusion tension imaging, DTI) is utilized to indirectly measure the differing degrees of anisotropy of water molecules in WM, GM and CSF. Anisotropy can be thought of as directional diffusivity. Measurements of anisotropy and isotropy can be used to estimate the structural characteristics of the cortex. Of the different brain tissues, diffusion in WM tends to be the most anisotropic (restricted along the axonal fascicles direction), less in GM, and least in CSF (unrestricted in all directions, or isotropic). Anisotropy in WM is thought to be influenced by cellular structures (e.g. axon diameter, myelination, organization and density of WM fibers) delimiting molecular motion.

A mathematical process called diffusion tractography estimates the direction of white matter bundles based on tensor orientation. White matter axonal bundles between cell bodies of neurons are commonly called fascicles; multiple grouped fascicles are called tracts. Tractography computationally represents fascicles and tracts as streamlines matching the diffusion orientation. All the streamlines estimated by tractography come together in a complex 3D model. This visual representation facilitates the understanding of the structural organization of human brain[15].

By applying a parcellation scheme to tractography, WM connections between different regions across the brain can be determined. This allows the calculation of structural brain connectivity (SC) metrics (e.g. further described in Chapter 3).

1.2.3 Functional MRI

During the 1990's, fMRI was established as a signal contrast mechanism based on T2*-weighted images, using blood oxygen level dependent (BOLD) contrast to examine brain activity by MRI scans[16,17]. Its use in basic neuroscience and clinical research has since increased significantly, owing in large part to its ability to non-invasively measure and map brain function over time[18].

It takes advantage of the differential magnetic susceptibility of oxyhemoglobin (diamagnetic) compared to deoxyhemoglobin (paramagnetic). When neurons increase their metabolic activity they first consume oxygen leading to deoxyhemoglobin increase, and then recruit more cerebral oxygenated blood leading to increased oxyhemoglobin presence in those regions (see for a review[19]). The ratio of oxyhemoglobin to deoxyhemoglobin allows measurements of the BOLD signal. Specifically, brain regions that show a low concentration of deoxyhaemoglobin give rise to a high BOLD signal. The magnitude of the BOLD signal, generated as a result of a task (i.e. task-fMRI) or by the brain at rest (i.e. resting-state fMRI), is considered to largely reflect neuronal activity or "brain activation". The BOLD signal measurement may also depend on pulsatility of arteries and veins, cerebral blood flow and volume, cortical morphology[20].

During task-fMRI acquisition the subject is asked to perform a task in the scanner. This allows the investigation of which brain regions present increased neuronal activity, presumably evoked by the task. This "brain activation" is captured by the correlation of changes in BOLD signal fluctuations with performance of the task compared to rest (i.e. baseline) across the fMRI acquisition session [21]. For example, a patient may be asked to perform a word generation task (or multiple similar tasks and/or trials) to map the brain regions involved in language generation (i.e. block-design). Since neuronal activity is not directly captured, a hemodynamic response function is used to model task-based changes in BOLD signal[22].

As opposed to task-based fMRI, resting-state fMRI evaluates the endogenous, spontaneous BOLD signal low-frequency fluctuations (< 0.1 Hz) in metabolic activity of the brain, while the subject is in a state of quiet wakefulness or watching a movie[23]. Resting-state fMRI functional connectivity (rs-FC) refers to the propensity of certain brain regions to behave similarly to each other over time. The assumption is that these regions serve related functions. This method uses linear temporal correlation between low-frequency fluctuations of BOLD signal at rest to determine the connection between two or more brain regions and/or brain networks[24].

Temporally correlated BOLD signal fluctuations have been shown to organize into canonical brain networks such as: salience network, auditory network, basal ganglia network, higher visual network, visuospatial network, default mode network, language network, executive network, precuneus network, primary visual network, and sensory motor network[25]. Importantly, these networks have been shown to correspond to functional maps derived from task-based fMRI where patients do sensory, motor or cognitive tasks[26]. Moreover, these networks are considered to reflect the intrinsic functional organization of the brain since they persist even under state of reduced consciousness (i.e. sleep, sedation, anesthesia) and/or pharmacological treatment.

In patients with epilepsy, rs-FC analysis allows identification and visualization of eloquent cortex and critical networks assisting the neurosurgeon in choosing the trajectory of resection with the least damage. For example, it is increasingly used for mapping language in epilepsy cases[27]. Since this technique does not require the patient to do a task, it is particularly useful in pediatric population, patients that are unconscious, and patients that cannot comply and/or follow the instructions for performing a task in the scanner. Moreover, as compared to task-based, resting-state fMRI takes less scanning time, does not need specialized personnel to assess the patient's neurocognitive status, and requires less complicated post-acquisition processing [22,23,25].

1.3 Thesis Outline

This thesis examines the relationships between the structure and function of the brain at the individual level in the context of aging and epilepsy. Generally, the anatomy of an

organ provides information about its behavior and function. This notion is limited when it comes to brain, despite the fact that most neurological conditions have an anatomical correlate. The unique inter- and intra-individual variability of the brain highlights the need for subject level, multimodal approaches in understanding brain functionality in health and disease. Gaining a better understanding of structure-function relationships through their fused visualization in Chapter 3, can help inform design and interpretation of basic neuroscience investigations in Chapter 2 and the advancement of clinical neurosurgical applications in Chapter 4.

1.3.1 Moderating Effect of Cortical Thickness on BOLD Signal Variability Age Related Changes

Dynamic changes in neuroanatomical structural and functional measures across the lifespan are commonly reported in association with aging. It is well established that normative aging is associated with structural changes in brain regions, and that these predict functional decline in various cognitive domains. However, the contribution of cortical morphology metrics such as cortical thickness (CT), cortical area (CA), and grey matter (GM) volume to age-related changes in brain function remain poorly understood.

Blood oxygen-level dependent signal variability, estimated using the standard deviation of the functional magnetic resonance imaging (fMRI) signal, or "$BOLD_{SD}$," is an emerging metric of variability in neural processing, and has been shown to be positively correlated with cognitive flexibility. Generally, $BOLD_{SD}$ is reported to decrease with aging, and is thought to reflect age-related cognitive decline. Nevertheless, the interaction between alterations in cortical morphology and $BOLD_{SD}$ changes has not been modeled quantitatively.

In this Chapter, we investigated the influence of cortical morphology metrics (i.e. CT, GM, CA) on age-related $BOLD_{SD}$ changes by treating these metrics as possible physiological confounds using linear mixed models. Specifically, we examined global and regional differences in $BOLD_{SD}$ in a group of older adults scanned twice at an interval of approximately 2.5 years, and regressed the effect of cortical morphology by introducing CT, CA and GM as covariates.

Results show that in our sample BOLD$_{SD}$ is confounded by CT. Respectively, changes in CT but not GM volume nor CA, show a significant interaction with BOLD$_{SD}$ alterations. Our study highlights that CT changes should be considered when evaluating BOLD$_{SD}$ alterations in the lifespan, providing insight into structure-function relationships in aging.

1.3.2 Visualization of Multimodal Brain Connectivity for Neurosurgical Planning using Augmented Reality

In neurosurgical procedures, precise preoperative planning requires extensive knowledge of the patient's anatomy as well as critical structures for brain function. An important consideration is weighing the risk of operating with that of post-surgical deficits. Recently, there has been an increase in the use of minimally invasive approaches, owing in part to advancements in multimodal medical imaging techniques such as structural (SC), and functional-based brain mapping (FC), which have been shown to be useful metrics for surgical trajectory planning. The main challenge associated with their use is the lack of intuitive structure-function visualization methods available to surgeons and trainees. Augmented reality (AR) represents a pivotal opportunity to overcome this limitation, by incorporating patient-specific structure-function brain data onto the user's vision of the real world.

In this study, we introduced a new mobile device AR application based on data derived from advanced image processing of multi-modal neuroimaging data. Advanced image processing was performed on multimodal neuroimaging data (T1- weighted image, DWI, rs-fMRI) to characterize the SC and FC of the brain. The AR application was designed to take these as inputs and allow the user to visualize and interact with the neuroanatomy in the context of its associated SC and FC. The performances of 10 users on 24 targets were evaluated using an extension of Fitts' methodology[28]. The users were able to use an interactive tool to select and visualize brain regions and their associated fibers. Results indicated that task difficulty increased as the volume of the fibers decreased, while movement time increased as task difficulty increased. Evaluation of the 3D pointing tasks showed consistency in user performance indicating its utility.

1.3.3 Presurgical brain mapping of the language network in pediatric patients with epilepsy using resting-state fMRI

Brain function is commonly represented in terms anatomical context. Epilepsy affects neural processing and often causes reorganization of brain function, causing localization of critical functions such as language based on anatomical landmark (i.e. Broca) alone difficult. Intra- and inter-hemispheric reorganization is more pronounced in children, due to their increased cortical plasticity. Surgery for intractable epilepsy (i.e. not controlled by medication) has the goal of achieving seizure freedom or reduction in seizure frequency while minimizing post-operative deficit in language abilities. Pediatric patients are often poor candidates for conventional brain mapping techniques (i.e. awake surgery, task functional magnetic resonance imaging, task-fMRI) as it is harder to get them to comply to the task. Rs-fMRI is an emerging presurgical brain mapping based on the intrinsic neural activity of the brain at rest with the potential to overcome the limitations of conventional mapping

In this study, we extracted language networks from rs-fMRI data in a cohort of young pediatric patients with epilepsy presenting for preoperative mapping by performing a similarity analysis with language network templates via a template-matching procedure. Rs-fMRI data was analyzed using independent component analysis, a data-driven method. Task-fMRI language mapping with verb generation and object naming was also performed. Language lateralization results from these two techniques were compared and good concordance was obtained in most cases. Ultimately, our results indicate that rs-fMRI can be a complementary method to obtain information for presurgical planning.

1.3.4 Conclusion

The structure and function of the brain are complementary and entwined aspects. Each can be investigated using equally entwined neuroimaging techniques and experimental paradigms. To this end, structure-function relationships in the brain were explored in the setting of basic neuroscience research on aging (Chapter 2) and epilepsy (Chapter 4) using multiple imaging methods, and visualization techniques such as AR (Chapter 3). Clinical relevance of the study of structure-function relationships in the brain, specifically

as it pertains to preoperative neurosurgery planning was discussed in Chapter 3 and Chapter 4.

<div align="center">Chapter 2</div>

2   Moderating Effect of Cortical Thickness on BOLD Signal Variability Age Related Changes

This Chapter is mainly adapted from:

D. R. Pur, R. A. Eagleson, A. de Ribaupierre, N. Mella, S. de Ribaupierre (2019): *"Moderating Effect of Cortical Thickness on BOLD Signal Variability Age Related Changes"* in Frontiers of Aging Neuroscience, 11. DOI:10.3389/fnagi.2019.00046

2.1   Introduction and relevant works

Normal aging is associated with marked functional and structural neuroanatomical alterations in cortical thickness (CT), gyrification, cortical surface area (CA), grey (GM) and white matter volume (WM)[29–31]. Therefore aging provides an interesting and dynamic framework to examine structure-function relationships of the brain.

Importantly, magnetic resonance imaging studies (MRI) show that the magnitude and rate of change of these cortical morphometry metrics is not constant across the cortex but rather it varies with age and brain region[4,32]. In fact, the relationship between cortical morphology metrics in aging is dynamic, with GM volume changes are reported to be largely accounted by changes in CT rather than CA, highlighting the importance of tracking changes in CT[4]. In fact, studies show that CT and CA are genetically independent[33]. Their neurodevelopment in the lifespan is largely independent of each other suggesting that they should be considered as separate metrics with different contributions to cortical volume[34]. Change in cortical morphology is reported to accelerate with increasing age. For example, a longitudinal study of alterations in cortical morphometry in older adults found accelerated changes with increasing age in temporal and occipital cortices[4]. Furthermore, other studies report that the temporal lobes are most vulnerable to age-related morphometric changes, and that these changes reflect age-related cognitive impairment[35,36]. There is considerable evidence that neuroanatomical alterations reflect underlying functional alterations, especially in cognition[37–39]. In fact,

functional magnetic resonance imaging (fMRI) studies, which rely on the blood oxygen level-dependent (BOLD) signal as a correlate of neuronal activity, report that changes in cortical morphology across adult lifespan impact the hemodynamic properties of the brain. For example, there are cortical laminar differences in BOLD signal[40], thicker cortical regions were reported to have a lower relative oxygen extraction fraction[41]. Therefore, since aging is associated with significant neuroanatomical alterations, these should be considered when assessing function (i.e. cognitive ability) using the BOLD signal.

The Standard Deviation of the BOLD signal can be used to estimate variability (hereafter, "$BOLD_{SD}$"), and is believed to reflect the brain's dynamic ability to undergo fast moment-to-moment switching through network reconfigurations[42,43]. It is an emerging index of cognitive health in aging, with higher regional $BOLD_{SD}$ being associated with enhanced performance on certain cognitive tasks (i.e. task switching) but not on others (i.e. distractor inhibition)[44]. Generally, increased $BOLD_{SD}$ is associated with younger age, faster and more consistent performance on cognitive tasks, and cognitive flexibility[44,45].

Nevertheless, the structural substrate and physiological mechanisms underlying $BOLD_{SD}$ remain largely unknown. For instance, decreased dopaminergic transmission is proposed to be associated with decreased $BOLD_{SD}$ in subcortical areas in older adults compared to younger ones[46]. However, there are few studies investigating the interaction between age-related alterations in cortical morphology and $BOLD_{SD}$. One study reported that increased microstructural integrity of WM pathways (measured as increased fractional anisotropy, FA) is associated with greater $BOLD_{SD}$[47]. FA, as measured by diffusion imaging is thought to reflect fiber density, fiber organization, axonal diameter, and myelination.

Given that neuroanatomical alterations associated with normative aging are known to influence cognitive performance, and that they influence the BOLD signal, their impact as physiological confounds to $BOLD_{SD}$ should be investigated. This is particularly relevant because there is a considerable degree of inconsistency of methods used and results across studies investigating $BOLD_{SD}$. In fact, some studies report greater

regional $BOLD_{SD}$ in older adults[42,48], individuals with stroke[49], Alzheimer disease[50] and other neurological disorders[51].

In this Chapter, we examined structure-function relationships of the brain by determining the contribution of cortical morphology metrics (i.e. CT, CA, GM volume) to brain function, represented by $BOLD_{SD}$ change, in a sample of older adults. A longitudinal framework, consisting of two scan points, should help reduce some of the inter-individual variance in neuroanatomy by accounting for external factors such as lifestyle, and various socio-economic and demographic factors.

We hypothesized that cortical morphology metrics show an interaction with $BOLD_{SD}$. We predict that age-related neuroanatomical alterations in CT, CA, GM are physiological confounds to $BOLD_{SD}$ measures, and that consequently adjusting for these metrics may help "unmask" the functional relevance of $BOLD_{SD}$.

2.2   Materials and Methods

2.2.1 Participants and MRI acquisition

All data obtained for the present study was obtained from the longitudinal Geneva Aging Study, after approval by the ethics committee of the Faculty of Psychology and Educational Sciences of the University of Geneva and the Swiss Ethic committee. Older subjects were initially recruited either from the University of the Third Age of Geneva or through newspaper and association advertisements for pensioners, as part of a larger longitudinal study. All participants gave written informed consent and older adults received a small amount of money as a compensation for their transportation fees.

Our initial sample consisted of 31 older adults scanned twice (mean age at first scan = 71.65 ± 6.03 years, mean age at second scan = 74.06 ± 5.99 years; 9 males). These subjects were chosen, within our pool, because they were the only ones that had undergone two T1 structural images and task fMRI scans, as well as other cognitive tests. Participants were screened for health problems with a questionnaire. The structural MRIs were inspected to rule out severe abnormalities (white matter changes, ventricular enlargement, tumours etc.). Three of the participants showed signs of Parkinson or lesion

on their anatomical MRI, so they were excluded from the final sample (n = 28). All models and results in this current paper thus reflect 28 older adults (mean age at first scan = 71.61 ± 6.21 years, mean age at second scan = 74.07 ± 6.15 years; 7 males). The scans were 2.46 ± 0.69 years apart.

Participants were scanned in a Siemens Trio 3T magnet. A BOLD fMRI task-rest sequence was administered using a reaction time paradigm, where the participant had to indicate on which side a cross was changing into a square, as fast as possible. The task consisted of eight experimental blocks, interspersed with eight resting/fixation blocks (respectively, 52 seconds – 20 seconds). The BOLD activity was obtained using an echo planar imaging acquisition (echo time, TE = 30 ms, time repetition, TR = 2100 ms, flip angle = 80°, field of view, FOV = 205 mm). Then, a structural T1-weighted MRI was acquired (TE = 2.27 ms, TR = 1900 ms, FOV = 256 mm, voxel size 1.0x1.0x1.0 mm).

2.2.2 MRI preprocessing and analysis

Structural T1-weighted MR images were analyzed using Freesurfer version 6.0, a widely used and freely available automated processing pipeline[2], which allows surface-based three dimensional reconstruction and quantification of cortical morphology. The standard steps for analysis were implemented (using "recon-all" pipeline with the default set of parameters). Regional measures of GM volume, CT and CA for each hemisphere were obtained using the automated anatomic parcellation procedure. Technical details are found in prior publications[52–54]. In brief, T1-weighted images underwent preprocessing steps including motion correction, brain extraction, intensity normalization, and Talairach transformation[55,56]. GM and WM surface boundaries were reconstructed to estimate the distance between them across the cortex[52]. The generated cortical models were inflated into spheres to be registered to a spherical atlas and parcellated into regions of interest using Destrieux atlas[52,57]. Change in cortical morphology between the two scanning sessions was determined as cortical morphology metrics GM (delta.volume), CT (delta.thickness), CA (delta.area) at timepoint 2–at timepoint 1.

---

[2] http://surfer.nmr.mgh.harvard.edu/

Processing of the functional data were performed using FSL version 5.0 (Analysis Group, FMRIB, Oxford, United Kingdom) [58]. Standard preprocessing were followed using FSL's FEAT and FSL's Melodic for functional data[59]. Briefly, for each participant preprocessing steps included motion correction, slice timing, spatial normalization, highpass temporal filtering (100 sec), smoothing (kernel 5 mm FWHM), and linear affine registration (12 degrees of freedom: 3 translations, 3 rotations, 3 shears and 3 zooms) of the functional data to the high-resolution T1 structural image, and from T1 to 1 mm standard space (MNI 152). Additionally, FSL's Melodic was used to regress signal from WM and CSF.

As part of the Geneva Dataset, the subjects were performing different cognitive tasks, and for the current study, only the fixation/rest blocks from the block design task fMRI were selected to calculate $BOLD_{SD}$, using a methodology previously described[42]. $BOLD_{SD}$ analysis was restricted to the GM using participant specific GM mask obtained from FSL's FAST. First, fixation blocks were normalized so that the overall four-dimensional mean (x*y*z*time) across brain and block was 100. Next, for each voxel, the block mean was subtracted to remove block-wise drift, followed by concatenation of all blocks. The standard deviation of the normalized mean of the concatenated fixation blocks was used to obtain $BOLD_{SD}$ values for each brain region (n = 148) of each subject, as defined by the Destrieux Atlas[57] using in-house MATLAB code. Change (delta.variability) in variability between the two scanning sessions was calculated as variability at timepoint 2 – variability at timepoint 1. $BOLD_{SD}$ encompassing both timepoints was introduced as "variability" (see Regional Model).

2.2.3 Statistical Analysis

Linear mixed effects models (LMMs) were used to investigate the potential confounding effect of cortical morphology, GM, CT, CA on $BOLD_{SD}$[60,61]. The LMMs allow estimation of the effects of explanatory variables ("fixed effects") and their interactions on the dependent variable (i.e. $BOLD_{SD}$), while statistically controlling for the effects of randomly selected participants ("random effects") on the dependent variable ($BOLD_{SD}$). Multiple models were run and the likelihood-ratio test was used to 1) investigate if introducing subjects as random effects improves the fit of the model 2) to

select the optimal combination of fixed effects fitted with maximum likelihood, while keeping the random effects structure the same. Therefore, the likelihood-ratio test via ANOVA was used to compare the goodness of fit of different models. R statistical software package (R Core Team, 2013) was used for all statistical analyses. Correlation between cortical morphology measures were computed using "cor" function in R. All models were fitted using the "lmer" or "lm" function in R. "lmerTest" R package was used to obtain summary table and p-values for linear mixed models via Satterthwaite's degrees of freedom method[62]. A spatio-temporal approach to LMMs allowed characterization of regionally specific variation across the brain[63]. This approach was implemented to investigate if there is a significant change in BOLD variability across time in all cortical regions, and if the change is region specific. Random effect structure with subjects varying in their "baseline" BOLD variability was retained (random intercept, 1|ID). Additionally, to model a different rate of change in the expected response levels, time varying predictors were introduced by random slopes (i.e. thickness, time) ("Regional Model"). To reduce spatial correlation issues an LMM model with the described structure was applied at each spatial location (i.e. region of interest) independently. Each model produced a parameter which quantifies the mean change in BOLD variability (delta.variability) for that region. P-values were corrected for multiple comparisons using false discovery rate (FDR) at q = 0.05[64].

Models

Model 1 = delta.variability ~ region

Model 2 = delta.variability ~ region+ (1 | ID)

Model 3 = delta.variability ~ delta.thickness + region+(1 | ID)

Model 4 = delta.variability ~ delta.area + region + (1 | ID)

Model 5 = delta.variability ~ delta.thickness + delta.area + region+(1 | ID)

Model 6 = delta.variability ~ delta.volume + region + (1 | ID)

Final Model = delta.variability ~ delta.thickness + region+ (1 | ID)

Regional Model = variability ~ time + thickness + (1+thickness + time | ID)

2.3 Results

2.3.1 Relations between cortical thickness and BOLD signal variability age-related changes

The functional and structural data of 28 participants was assessed. As expected, our study showed that CA and GM volume are highly correlated r = 0.904, p < 0.001 (95% Cl 0.901 – 0.908) and consequently collinearity was suspected. Multiple LMMs were utilized to assess the effect of neuroanatomical metrics CT, CA and GM on $BOLD_{SD}$ age-related changes. Results from the linear mixed effect models run with likelihood-ratio test via ANOVA, are presented in Table 2-1**.** A) indicates that subject intercept should be introduced as a random effect, while B) C) D) E) show the steps that have led to the final model. Specifically, Table 2-1. B) and C) indicate that introducing CT or CA as covariates, separately, each significantly improve the fit of the model p < 0.0001, p < 0.05, respectively. However, from D) it is apparent that adding CA to a model that already has CT as a covariate does not improve the fit of the model, meaning that CT only should be included in the final model (see "Final Model"). E) indicates that introducing GM as a covariate does not improve the fit of the model. Neither CT, GM nor CA mean changes were significant as tested with LMMs. Regional Model LMM indicated that neither overall nor regionally specific mean $BOLD_{SD}$ change was significant after FDR correction.

Abbreviations: Df, degrees of freedom; AIC, Akaike information criterion; BIC, Bayesian information criterion; logLik, log-likelihood; Chisq Chi, Chi-Square test statistic; Pr > Chisq. P < 0.05. ID represents subject identification number.

Table 2-1 Results from likelihood-ratio test via ANOVA for model comparison.

(A) Determine if random effects for subject intercept should be introduced:

Model 1	delta.variability ~ region							
Model 2	delta.variability ~ region + (1|ID)							
	Df	**AIC**	**BIC**	**logLik**	**deviance**	**Chisq Chi**	**Df.**	**Pr > Chisq**
Model 1	149	-2771.9	-1828.8	1534.9	-3069.9			
Model 2	150	-3744.8	-3744.8	2022.4	-4044.8	974.97	1	< 2.2e-16

(B) Determine if introducing thickness as a covariate improves the goodness-of-fit:

| Model 2 | delta.variability ~ region + (1|ID) |
| Model 3 | delta.variability ~ delta.thickness + region + (1 | ID) |

	Df	AIC	BIC	logLik	deviance	Chisq Chi	Df.	Pr > Chisq
Model 2	150	-3744.8	-2795.4	2022.4	-4044.8			
Model 3	151	-3765.5	-2809.8	2033.8	-4067.5	22.691	1	1.903e-06

(C) Determine if introducing area as a covariate improves the goodness-of-fit:

| Model 2 | delta.variability ~ region + (1 | ID) |
| Model 4 | delta.variability ~ delta.area + region + (1 | ID) |

	Df	AIC	BIC	logLik	deviance	Chisq Chi	Df	Pr > Chisq
Model 2	150	-3744.8	-2795.4	2022.4	-4044.8			
Model 4	151	-3749.0	-2793.3	2025.5	-4051.0	6.2025	1	0.01276

(D) Determine if introducing both area and thickness as covariates as compared to just
   one improves the goodness-of-fit

| Model 3 | delta.variability ~ delta.thickness + region + (1 | ID) |
| Model 5 | delta.variability ~ delta.thickness + delta.area + region + (1 | ID) |

	Df	AIC	BIC	logLik	deviance	Chisq Chi	Df.	Pr > Chisq
Model 3	151	-3765.5	-2809.8	2033.8	-4067.5			
Model 5	152	-3766.7	-2804.7	2035.4	-4070.7	3.2151	1	0.07296

(E) Determine if introducing GM volume as covariate improves the goodness-of-fit:

| Model 2 | delta.variability ~ region + (1 | ID) |
| Model 6 | delta.variability ~ delta.volume + region + (1 | ID) |

	Df	AIC	BIC	logLik	deviance	Chisq Chi	Df.	Pr > Chisq
Model 2	150	-3744.8	-2795.4	2022.4	-4044.8			
Model 6	151	-3743.1	-2787.3	2022.5	-4045.1	0.2245	1	0.6357

2.4 Discussion

2.4.1 Cortical Thickness and its Association with BOLD$_{SD}$

In this study we aimed at determining the contribution of cortical morphology to
BOLD$_{SD}$ in order to better understand structure-function relationships in the brain.

BOLD$_{SD}$ changes across the lifespan have been shown to be robust to certain vascular
factor such as cerebral blood flow, BOLD cerebrovascular reactivity, maximal BOLD

signal change[65], as well as GM volume changes[48]. However, using LMMs, we found that functional alterations in aging as captured by $BOLD_{SD}$ are confounded by the structural metric CT. This is not surprising, considering that it is well known that BOLD signal change/activation is dependent on the laminar organization of the cortex, and consequently is influenced by its depth or thickness[40,66,67]. In fact, neurovascular coupling is reported to vary by cortical depth and layer[68].

In a longitudinal study investigating CT, GM volume, CA across the lifespan, Storsve et al. (2014) reported cortical morphology metric specific and region specific rates of mean annual percentage change (APC) in healthy adults aged 23-87 years. In most regions, GM volume has a mean APC of – 0.51%, CT of -0.35%, CA of -0.19%. Other longitudinal studies in older adults, report similar reductions: in GM volume, mean APC ranging from - 0.5% to - 2.1% ± 1.6%[35,69] in CT, mean APC –0.3%[70]. In our sample, the change in cortical morphology from scan 1 to scan 2 (2.5 years apart) was not statistically significant. However, the findings reported by these longitudinal studies suggest that while the neuroanatomical alterations may be too subtle to reach statistically significance in the investigated timespan of 2.5 years, they may still contribute to $BOLD_{SD}$ age-related findings. Particularly, accounting for CT age-related changes may help "unmask" the functional value of $BOLD_{SD}$.

The hemodynamic properties of each brain region are highly correlated with its cortical structure[20,41]. Thicker regions show decreased neuronal density, and higher concentration of glial cells and synapses relative to neurons. Thicker areas tend to extract less oxygen from the blood, as measured by oxygen extraction ratios (i.e. expressed as local-to-global ratio). These findings indicate that laminar differences in cellular content impact neurovascular coupling mechanisms, which in turn may compromise the power of $BOLD_{SD}$ measurements to detect "real" changes in neuronal variability processing. Although, laminar differences in $BOLD_{SD}$ remain rather elusive, our study suggests the that CT should be considered in BOLD variability studies.

2.4.2 Age-related changes in BOLD$_{SD}$

In our study we did not find a significant change in BOLD$_{SD}$, likely due to the low timespan between scans (2.5 years), and relatively low sample (n = 28). Overall, most studies reporting a decrease in BOLD$_{SD}$ suggest that this finding may indicate structural reductions in synaptic complexity and integrity, as well as functional decline in neural optimization and flexibility[42]. Burzynska et al, (2015) reported a positive correlation between increased microstructural integrity of WM and BOLD$_{SD}$ in healthy adults, consequently warranting the consideration of structural alterations in variability studies.

Two seminal studies investigated BOLD$_{SD}$ differences in aging alone[42] and in relation to performance on cognitive tasks[71] between a young group of participants (20-30 years) and an older one (56-85 years) and found both increases and decreases in regional variability with younger age alone, and younger age and better performance making it rather difficult to isolate specific key contributing regions. Most regions in these two studies showed the same trend but there were some inconsistencies. For example, superior frontal gyrus was reported show greater variability with younger age and better performance in one study, while another one reported that its variability increases with age. CT was not considered in any of these studies.

The relationship between cognitive performance and/or flexibility and BOLD$_{SD}$ is definitely complex and task dependent. Behavioral studies indicate age-related differences in intra-individual variability on cognitive performance tests involving reaction time, and working memory. Older adults showing higher intra-individual variability on reaction time tests than younger adults, while the opposite is observed on working memory tests[72].

2.4.3 Possible confounds in BOLD$_{SD}$ studies

Most studies investigating BOLD variability utilized a cross-sectional design while we used a within-subject design. This design is a highlight of our study because it allows for the investigation of normative age-related differences, specifically intra-individual effects of the processing of aging on cortical morphology and BOLD$_{SD}$, rather than simply age differences across groups. Importantly, the within-subject design helps account for

numerous sources of individual differences that may affect BOLD variability such as differences in dopaminergic neurotransmission[46] and even differences in tendency for financial risk taking[73]. Given that in our study the participants were scanned at an interval of approximately 2.5 years, we were able to at least partially account for such factors. Furthermore, it is clear from the literature that there are numerous lifestyle factors (i.e. socioeconomic status, education) that may contribute to individual neuroanatomical alterations, which in turn may confound BOLD variability studies[74]. This further supports the findings of our study, specifically that CT is a neuroanatomical metric that should be accounted for.

Lastly, there may be inconsistency in results between studies due to: 1) using task-fMRI and resting-state fMRI, 2) calculation of BOLD signal variability using standard deviation vs mean-square successive difference) (for review, Garrett et al., 2013), 3) type of statistical analysis performed (e.g. partial least squares method, LMM, general linear model) 4) not accounting for contribution of CT and the other mentioned sources of individual differences.

2.4.4 Limitations

The main limitation, as discussed above and further addressed by Garrett et al. (2013), Scarapicchia et al. (2018), are the lack of standardization in acquiring and analyzing the fMRI data. Additionally, the sample used in our study consists of a relatively small sample of older adults and rather short scan-rescan time, consequently this limits our ability to make strong generalization to other age groups or longer time spans, respectively. Nevertheless, since studies show that the brain undergoes extensive annual structural alterations across the lifespan at different rates, our finding that CT contributes to $BOLD_{SD}$ alterations, remains an important consideration.

2.5   Conclusion

In conclusion, this Chapter indicated that structure-function relationships in the brain are an important consideration in the design and interpretation of neuroscience studies. Contrary to a view that BOLD variability is just "noise", we consider it to be emerging as an important metric of normal aging. Keeping in mind that across the lifespan there are

considerable cortical morphometry alterations and that cortical depth affects the BOLD signal, we reported that cortical thickness contributes to BOLD$_{SD}$ changes, in an older sample of health adults.

Chapter 3

3 Visualization of Multimodal Brain Connectivity for Neurosurgical Planning using Augmented Reality

This Chapter is adapted from:

D. R. Pur, D. Kikinov, S. de Ribaupierre, R. A. Eagleson (2019): "*Visualization of Mutimodal Brain Connectivity for Neurosurgical Planning using Handheld Device Augmented Reality"* in Proceedings of the 5th World Congress on Electrical Engineering and Computer Systems and Sciences (EECSS'19), 126. DOI: 10.11159/icbes19.126

3.1 Introduction

Visualization of multimodal brain connectivity in the form of functional (FC) and structural connectivity (SC) allows the investigation of structure-function relationships in the brain in an intuitive way. One major application beside studies basic neuroscience is in preoperative planning for neurosurgery.

Numerous neurosurgical procedures require extensive multimodal preoperative brain mapping for identification of a precise surgical trajectory that will spare eloquent cortex (i.e. cortex that if damaged will lead to severe neurological deficits). The introduction of minimally invasive surgeries, which require a small "keyhole" entry point into the skull, further emphasizes the need for the surgeon to be able to preoperatively visualize and interact with relevant brain structures to safely plan the neurosurgical trajectory. In this setting, understanding and visualizing structure-function relationships is crucial.

Conventionally, surgeons are required to do cognitively demanding mental transformations to coordinate between preoperative two-dimensional (2D) patient-specific magnetic resonance images (MRI) and patient reference frames (i.e. three-dimensional, 3D, anatomy) [75]. Additionally, they need to adeptly manipulate instruments in the surgical field while looking at a 2D display of preoperative images[76]. This is

particularly challenging in the case of junior trainees who may have limited previous surgical experience and less developed spatial and perceptual intuition. Ultimately, this leads to longer surgeries and increases the chance of error associated with reduced performance due to cognitive overload[75].

Augmented reality (AR) incorporates patient-specific virtual preoperative data onto the user's vision of the real world[76,77]. Medical applications of AR are on the rise in various fields of medicine both surgical (e.g. trajectory planning, training) and non-surgical (educational, psychiatric or psychological treatments). These have been extensively reviewed previously. [78–81]. AR use in neurosurgery includes AR systems for surgical planning, surgical navigation, or surgical training. These feature various methodologies and implementations (e.g. head-mounted display, augmented monitors, augmented optics) [82,76]. Related work to *NeuroAR,* includes AR presurgical planning simulators aimed at facilitating training and planning of surgeries prior to the actual procedure, such as *ImmersiveTouch*[83,84], a wearable Hololens device[85], mobile device AR applications [86,87] (for review see[82,88]). However, the majority of existing neurosurgery AR systems are devoted to intraoperative use for tumor resection, open neurovascular surgery, ventriculostomy, or spinal surgery[76]. Additionally, in contrast to *NeuroAR*, none of the surveyed systems made use of advanced image processing techniques to derive and display FC and SC information. The benefit of using multimodal brain connectivity measures in brain mapping is well established [89]. Therefore, FC and SC image fusion display in AR is of particular interest because it not only adds visuospatial context but it also has the potential to provide information about the importance of different brain areas based on preoperative scans (i.e. eloquence scores)[90,91].

In this Chapter, we introduce a mobile device AR system, *NeuroAR*, designed and evaluated with human factors in mind, which allows real-time, intuitive, 3D visualization and interaction with brain structures and multimodal brain connectivity to facilitate training for neurosurgical procedures. Specifically, the individualized identification of eloquent cortex is facilitated by our system which displays both patient specific brain structural connectivity (SC) and functional connectivity (FC), as well as anatomical landmarks derived from MRIs. To evaluate the performance of the AR application, we

extended Fitts' methodology and applied to a 3D pointing task guided by a 3D environment, presented on a mobile device screen (i.e. 2D display).

3.2 Materials and Methods

3.2.1 MRI acquisition and preprocessing

A functional resting-state fMRI (rs-fMRI) (TE = 27 ms, TR = 2100 ms, flip angle = 80°, FOV = 200 mm), structural T1-weighted image (time echo [TE] = 2.27 ms, time repetition [TR] = 1900 ms, field of view [FOV] = 256 mm, voxel size 1.0x 1.0 x1.0 mm) and diffusion weighted image, DWI (TR = 8400 ms, TE = 88 ms, b value = 1000 s/mm2, and voxel size $2.0 \times 2.0 \times 2.0$ mm) were acquired from a healthy participant (30 years old, female). All the scans were acquired using a Siemens Trio 3T magnet.

The MRI data were processed and then used as inputs in the AR application. The T1-weighted image was analyzed using Freesurfer (v5.3) automated processing pipeline[3] to obtain the topological representation of the GM (i.e. cortical brain regions) in the form of a mesh brain surface. The standard steps for processing were implemented: motion correction[56], brain extraction using a watershed/surface deformation procedure [92], affine transformation (12 degrees of freedom) to the Talairach image space, non-uniform intensity normalization[55]. The brain was segmented into white matter (WM), GM, and cerebrospinal fluid (CSF). Next, surface deformation following voxel intensity gradients to optimally place the grey/white and gray/CSF borders at the location where the greatest shift in intensity defines the transition to the other tissue class are performed to create a 3D surface model of the brain [12,52,93] (Figure 3-1). Freesurfer's Desikan-Killiany Atlas was used to characterize the brain regions used in this study[94].

---

[3] http://surfer.nmr.mgh.harvard.edu/
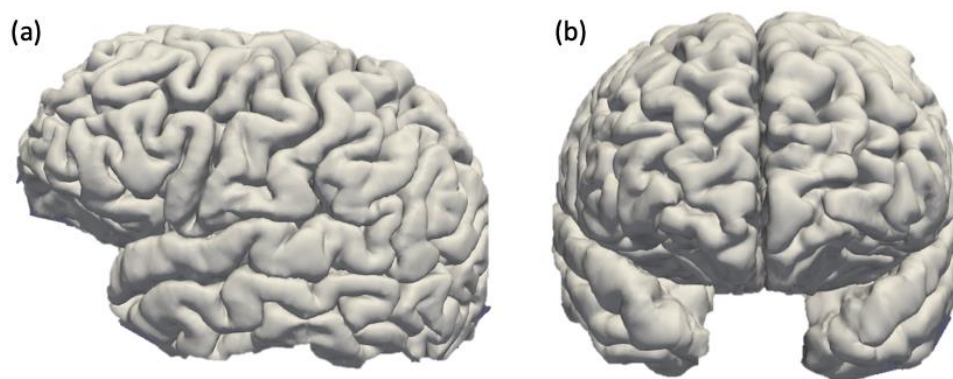
Figure 3-1 3D model of the brain obtained from FreeSurfer. Different views are presented: (a) sagittal, (b) coronal

Next, 3D Slicer (v4.9)[4] module Model Maker was used to create individual 3D surface model of each brain region using each region's boundaries via a marching cube algorithm. The DWI was processed with FSL "topup" and eddy current correction to reduce artefacts (FSL version 5.0; Analysis Group, FMRIB, Oxford, United Kingdom). 3D Slicer modules DWI to DTI Estimation and Tractography Label Map seeding were used to generate fiber tracts of the WM (i.e. tractography) as VTK[5] files using the DWI image (Figure 3.2). The algorithm matching brain regions to their WM fibers is based on MultiXplore[6], a scriptable module which can be added to 3D Slicer, previously discussed by Bakhshmand et al., (2017)[91]. First, to generate the SC matrix using MultiXplore, the number of WM fibers (i.e. modelled as streamlines) was calculated for each pair of cortical brain regions. The WM fibers were clustered based on their intersection with cortical brain regions. The brain regions were nodes and the number of streamlines were edges in the SC matrix.

---

[4] http://slicer.org

[5] https://www.vtk.org

[6] http://www.nitrc.org/projects/multixplore/
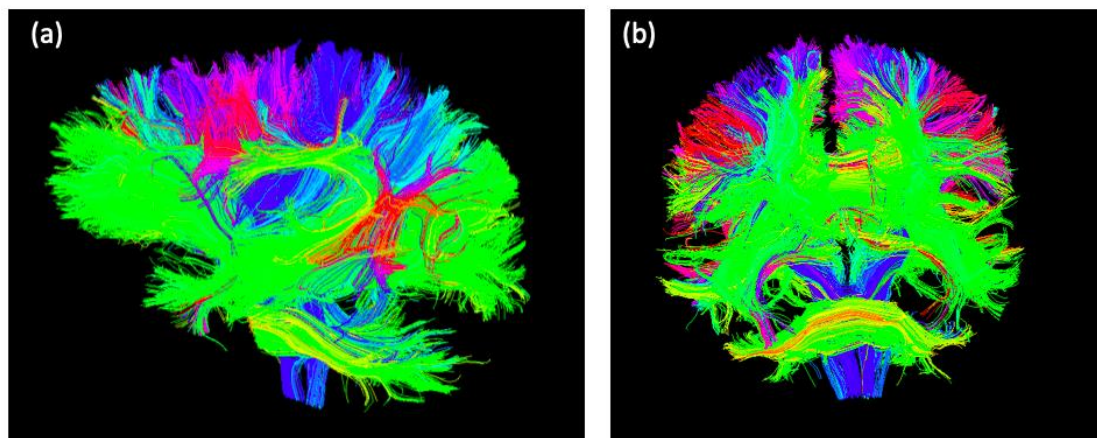
Figure 3-2 Tractography obtained with 3D Slicer, with (a) sagittal, and (b) coronal view.

The average of fMRI signals in each brain region, as indicated by the Desikan-Killiany atlas, was extracted from the pre-processed rs-fMRI using a pipeline consisting of tools from FSL and Niftireg[7]. FSL was used for standard pre-processing steps: motion correction, slice timing, spatial normalization, high pass filtering (100 sec), smoothing (kernel 5 mm FWHM), regression of signal from WM and cerebral spinal fluid. NiftiReg[6] was used to register the Desikan-Killiany parcellation of the T1-weighted image previously obtained to the functional data.

The average fMRI signals of each brain region were used to derive the FC matrix using a MATLAB script described in Bakhshmand et al., (2017) based on dynamic FC method (time window = 30 scans).

3.2.2 Augmented Reality Processing

For the 3D rendering of augmented reality, Unity[8] was used with Vuforia Engine (Unity: v2018.1.0, Vuforia: 7.2.24), any Android device running Android 7.0 or higher; tested on Samsung Galaxy S8+, and Samsung Galaxy Tab S2. Given the VTK file format, a Unity-compatible model had to be generated. This was done manually, by using

---

[7] http://cmictig.cs.ucl.ac.uk/wiki/index.php/NiftyReg

[8] http://unity3d.com

Paraview[9] to change each VTK file into a .x3d file and then through Blender[10] by importing the .x3d files and exporting them as .obj files. To ensure WM fiber visibility, in Blender, the bevel attribute of the shape's geometry was adjusted (between 0.01 to 0.1). Each model was individually brought into Unity and grouped together. For each fiber tract a button was created and connected to a brain region based on determined SC. These buttons were then added the functions to show or hide the associated fiber and connected regions. The FC matrix was also imported into Unity where it was parsed and saved during runtime. Using the parsed matrix data, the buttons for each fiber bundle were then coloured based on the correlation/connectivity strength of the two regions in the matrix, with dark red being at 1, green at 0, dark blue at -1, with in-between values being coloured along a gradient. A new Unity material with a custom vertex normals shader was created for use on the fibers. For each vertex, their normal was calculated and then translated into a colour: an RGB value between 0 and 1. This gives the fibers a distinct colour based on their three-dimensional direction.

3.3 Uses

The user has many options on screen to choose from a) show, hide all the WM fiber tracts with their associated brain regions, b) individually show, hide WM fiber tracts, c) visualize the tractography (all WM fiber bundles) within the brain surface mesh or by itself, d) show, hide transparent brain surface mesh of the left and right hemispheres (Figure 3-3). The background of the buttons on the menu are coloured based on FC. With these options the user is able to visualize as much of the tractography as they want, with or without the associated brain regions, and isolate certain clusters of brain regions of interest in the participant's brain. There is also an option for the user to see which features are connected via interaction, where they can use an interactive tool to select different brain regions or the WM fibers between them.

---

[9] https://www.paraview.org

[10] https://www.blender.org

Specifically, the user can use an interaction tool to touch the augmented model. If the tool comes into contact, via Unity's built-in collision detection system, with any WM fiber bundles it will highlight the contacted fibers as well as their source brain regions in yellow. This allows the user to physically test surgical paths and view which areas would be affected. The user can only interact with shown tractographies (Figure 3-3).
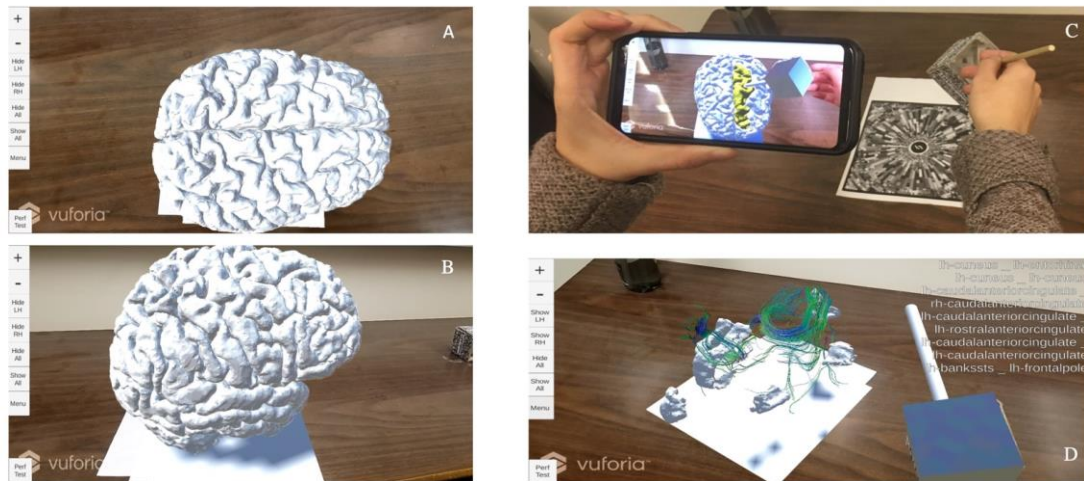
Figure 3-3 The user's view through the mobile screen of the AR application. The user can explore the neuroanatomy and structural connectivity of the brain using the tool. A) Axial view of the cortical surface mesh model of cortical grey matter. B) Sagittal view of the cortical surface mesh model of cortical grey matter. C) Depiction of user selecting a brain region on the cortical surface mesh model using the interactive tool. Region selected is yellow. D) View of the user exploring the structural connectivity between various regions (listed on the left side of the figure). The full model is hidden and only the brain regions selected are shown.

Figure 3-4 The user's view through the mobile screen of the AR application including the menu. The user can explore the neuroanatomy and both the structural and functional connectivity of the brain using the tool. Background of the buttons indicate the strength of the functional connectivity between the regions -1 strong negative, +1 strong positive. The user can explore these functionalities using the scroll bar.

3.4   Experiment

All procedures performed in the study involving human participants were in accordance with the ethical standards of the ethics committee of the Faculty of Psychology and Educational Sciences of the University of Geneva and the Swiss Ethics committee, and with the 1964 Helsinki declaration and its later amendments. Informed consent was obtained from all individual participants included in the study.

Ten subjects participated in the experiment. The participants were university graduate students or undergraduate students. They all had normal or corrected-to-normal vision. All participants were novices in using AR devices and had minimal to no neuroanatomical knowledge. Therefore, 1 training trial was performed before engaging in the test tasks.

A study consisting of a pointing task was used to evaluate the performance achieved by the AR application. Studies indicate that Fitt's law[28], a mathematical model used to describe the relationship between target size, distance, and movement time is a validated method for evaluating graphical interfaces and pointing tasks. First, an index of

difficulty (ID) was calculate for each fiber tested, to evaluate the difficulty of the pointing task. Index of performance (IP) was used to calculate movement time based on ID to indicate human performance. Human performance is defined as a trade-off between accuracy and speed.

$$ID = \log_2(2A/W)$$

(1)

Where A is the distance between the center of the start cube and the center of the fiber, and W is the volume of the fiber.

$$IP = \frac{ID}{MT}$$

(2)

Where ID is the index of difficulty and MT is the movement time for the task.

Unity with Vuforia were used for augmented reality rendering (Unity: v2018.1.0, Vuforia: 7.2.24), testing was done on Samsung Galaxy S8+ (Figure 3.5). Basic instructions about navigating the AR environment were given to the users. The users had a trial run to get comfortable using AR tool. Once the users were comfortable with interaction between the tool and the fibers, the testing began.

Briefly, the users had to push a button "Perf Test", use the tool to collide with an AR cube, use the tool to touch the fiber, and finally touch any point on the screen when they were confident with their interaction. Upon clicking the button, the menu was hidden from the user, a WM fiber bundle was isolated along with the brain regions it connects and the start cube was generated. Besides touching the WM fiber and the cube nothing else can be done, limiting random mistakes from users. Once the user touches the cube, it disappears giving the user the visual cue that the test has begun, where they are expected to touch the fiber; at this point data collection begins. When the user was certain they touched the fiber, they had to tap the phone screen with their finger, ending the data collection and the test for that fiber. This screen tap can only be done after the start cube has been touched, meaning that the user could not accidentally end the test before it began. The user repeated the process for 24 WM fibers which were all logged. Once all

the data had been saved, the original menu reappears signalling to the user that they have completed the task.

Each frame, the position (3D, x, y, z in units used by Unity) and orientation (quaternion, w, x, y, z) of the needle relative to the fiber was logged, along with the time stamp. This resulted in position and orientation data being recorded about 60 times per second. Once the user completed the task by tapping the screen, the positional and orientation data was saved as a CSV file with the associated task's number. Upon completion a second CSV file was generated which had the name of the fiber in the task, the calculated distance of the fiber from the start cube, the volume of the fiber and the total task time (time recorded at the end, subtracted by the start time). The volume of the
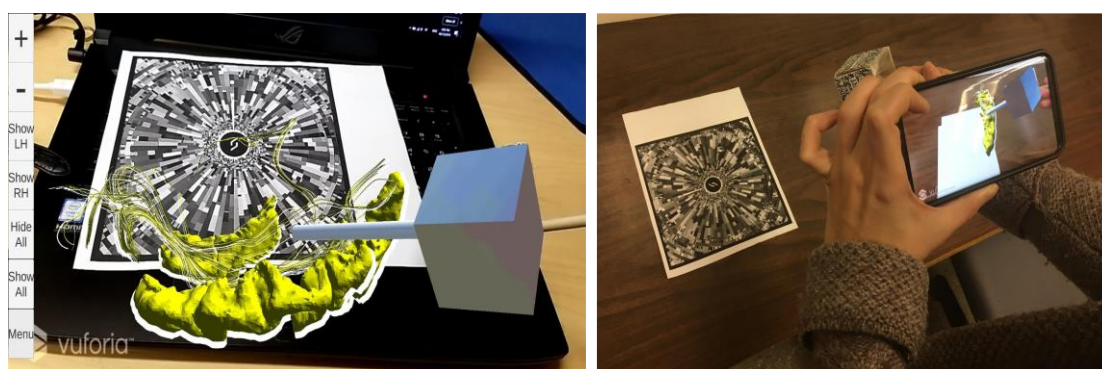
fiber was calculated using the triangles and vertices of the fiber's mesh, resulting in larger fibers having larger volumes.

Figure 3-5 The user's view during the pointing task through the mobile screen of the augmented reality application. *Show LH,* show left hemisphere; *Show RH*, show right hemisphere; *Hide All*, hide all brain regions; *Show All,* show all brain regions; Menu takes the user to the functional connectivity buttons.

The test duration was approximately 15 minutes.

3.5 Results

When using the AR application, anatomical detail (brain regions/structures) from the segmented T1-weighted image was able to be fused with a) the SC obtained from the processed DWI scan in the form of WM fiber bundles, b) the FC obtained from the processed rs-fMRI in the form of color-coded buttons in the scroll menu. The buttons link

two cortical brain regions. Table 3-1 presents the results of the pilot user performance experiment (see Appendix A. for results at all targets).

Table 3-1 Results of users at the first 5 targets. For each pointing task/fiber target, the average and standard deviation of the performance of all subjects at that task was calculated. The volume and index of difficulty were constant across subjects and varied per task. MT, movement time; IP, index of performance; Volume, volume of the fibers; ID, index of difficulty.

Task no.	MT (seconds) Avg	SD	IP (bits/seconds) Avg	SD	Volume (u^3)	ID (bits)
1	3.397	± 1.302	1.698	± 0.521	0.009224	5.198
2	7.787	± 3.745	1.653	± 1.257	0.000541	9.301
3	5.233	± 5.047	3.155	± 1.524	0.000199	10.777
4	3.318	± 1.601	3.316	± 1.247	0.000501	9.448
5	9.451	± 8.205	2.324	± 2.120	0.000128	11.403

A)

Average User Movement Time per Index of Difficulty

B)

Index of Difficulty Per Volume Target

Figure 3-6. Relationships between indices calculated according to Fitts' Law. The values plotted represent the average response of the participants at each of the 24 targets. A) Plot indicates average user movement time as it relates to index of difficulty for each target attempted. Pearson's correlation coefficient was calculated as $r = 0.22$. X-axis represents index of difficulty (bits), Y-axis represents movement time (seconds). B) Plot represents the relationship between task difficulty and volume of targets. Pearson's correlation coefficient was calculated as $r = -0.82$. X-axis represents volume (u^3), Y-axis represents index of difficulty (bits).

Overall, our data showed that there was relatively good consistency in the responses of the users. As task difficulty increased so did MT, depicted in Figure 3-6 A). Pearson's correlation indicated a low positive correlation between MT and ID, r = 0.22. As the volume of the WM fibers increased task difficulty decreased, depicted in Figure 3-6 B). As expected, Pearson's correlation indicated a strong negative correlation between volume of target WM fibers and ID, r = -0.82.

Based on the results of the performance test, the users found the application useable. Performance was better and more consistent at some targets (e.g. 7, 1, 9) than others (5, 20, 16) (see Figure 3-7).
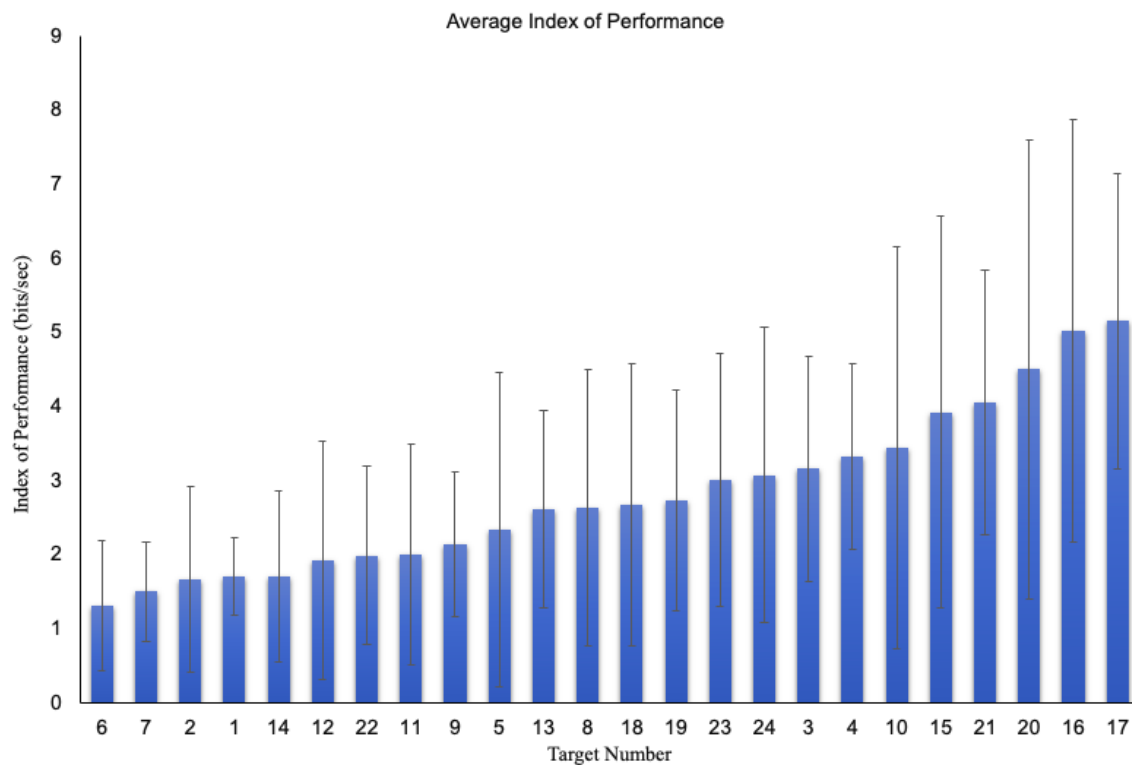
Figure 3-7. Average index of performance across the 10 users per pointing task/fiber target (n = 24). Targets were sorted on the X-axis in ascending order based on the value of the index of performance. Error bars represent the standard deviation of the average index of performance

3.6 Discussion

Our mobile AR implementation allows user friendly visualization and exploration of multimodal brain connectivity in the context of anatomical landmarks. Intuitive incorporation of brain connectivity in the form of SC and FC in the preoperative plan can help the surgeon choose a surgical trajectory that minimizes the risk of post-operative deficit. Furthermore, visualization of brain connectivity in AR facilitates the study structure-function relationships at the level of the individual.

We implemented a pointing task experiment to evaluate the performance and usability of the AR application. There was a weak positive linear relationship between the difficulty of the task (i.e. ID) and MT required to complete it (r = 0.22), depicted in Figure 3-6., A). The assumption is that as the difficulty of pointing to the WM fiber targets increases so does the time to mentally choose a trajectory and to execute the movement. There are several factors that may have contributed to a relatively low correlation. Notably, there were differences in the way users approached the targets. For example, some choose a trajectory and stuck to it while others changed their mind as they approached the target. Moreover, MT may have also been affected by sporadic issues with tracking of the tool. There was a strong negative correlation between task difficulty and volume of the WM fiber target (r = -0.82), depicted in Figure 3-6., B). Very small targets were the most difficult to touch. As their volume increased the difficulty decreased, likely because they were more easily identified on the display of the mobile device. The overall trends presents in Figure 3-7. shows the average performance of the users as it relates to target number. User performance was similar across the different targets, confirming the usability of the application. Unexpected peaks in performance can be attributed to user error, as some users accidentally ended the task without touching the fiber or lost tracking of the tool, which led to higher standard deviation (most notable at task 2, 5, 10, 20).

3.7 Conclusion

In this Chapter, we examined brain structure-function relations through visualization of multimodal brain connectivity using augmented reality. In terms of clinical applications,

AR visualization and interaction with preoperative multimodal brain connectivity allows the surgeon to safely explore the patient anatomy and identify eloquent cortex based on advanced image processing, as well as try different neurosurgical approaches prior to surgery. Furthermore, our tool can also be used as a potential educational model for neurosurgical residents and medical students for neurosurgical planning. When tested amongst a pilot group of students, the users found the application useable and were able to interact with both small and large fibers without any issues. As expected, when targeting fibers with higher indices of difficulty, the movement time of the users increased, which is consistent to the extended Fitts' methodology

Chapter 4

4 Presurgical brain mapping of the language network in pediatric patients with epilepsy

4.1 Introduction

Epilepsy affects neural processing and often causes reorganization of language networks through multifactorial age-dependent cortical plasticity[7]. Surgery in select cases of children with pharmaco-resistant focal epilepsies can significantly improve their quality of life and cognitive outcomes by providing them with seizure freedom or a period of reduced seizure frequency during critical periods of childhood development[95,6,96].

Preoperative assessment of language localization is necessary to evaluate and minimize the risk of post-operative deficit. Brain mapping to determine the brain regions involved in language functioning is critical in children with epilepsy because they often present with an atypical pattern for language. Both inter-hemispheric and intra-hemispheric language network reorganization are common in the setting of pediatric epilepsy [97,98,99].

The clinical gold standard procedures for mapping eloquent cortex, direct cortical stimulation (DCS), either from subdural grids and electrodes or stereoelectroencephalography (SEEG) during an invasive monitoring at the bedside, or in the operating room with a stimulator, require staged surgery with mapping done at the bedside or awake surgery. These invasive techniques have the benefit of being highly specific (i.e. show only areas critical for language)[7] but are technically challenging (e.g. require large area to interrogate) and carry non-trivial risks for complications associated with electrode placements[100,101]. It is more difficult to obtain results in children than adults during stimulation because of their inability to comply due to age or cognitive delay and their neurophysiology – higher stimulating thresholds[6,102].

Functional magnetic resonance imaging (fMRI), indirectly measures neuronal activity by analyzing fluctuations in the blood oxygen level dependent (BOLD) signal in

response to a task (task-fMRI) or at rest (resting-state fMRI), and is increasingly used as a non-invasive language mapping alternative with relatively good concordance with conventional methods[7,103,104]. Task-fMRI requires the performance of several language tests (e.g. verb generation, picture naming) each aimed at capturing distinct aspects of expressive and receptive language. The quality of the output depends on adequate performance on multiple demanding tasks making it relatively impractical in younger children and/or children with language deficits/delays caused by the epilepsy, even though mapping is critical in these very patients. Therefore, task-fMRI shares same of the same limitations as stimulation techniques.

Recently, resting-state fMRI (rs-fMRI), a non-invasive, "task-free" technique based on low-frequency temporal correlations of BOLD signal at rest[24], has shown potential to overcome these limitations. The language network is one of the resting-state networks (RSN) that can be obtained by applying functional connectivity analyses to rs-fMRI data. Interestingly, there is evidence that RSNs and task-fMRI activation maps show similar topologies with high correspondence, suggesting that task activation is already contained in the more comprehensive rs-fMRI data[105].

Several studies have investigated its use in presurgical planning in adults with epilepsy or brain tumors, with favorable concordance with conventional methods[106,107]. Even though there are limited reports of rs-fMRI brain mapping in pediatric epilepsy cases, the results are promising and warrant further investigation. Comparable localization was reported when comparing rs-fMRI maps with stimulation sites for sensorimotor mapping[108], and rs-fMRI maps with task-fMRI maps for language[109]. Past studies investigated its applicability through case series of children with various pathologies including epilepsy[110111], while others have assessed its potential to be integrated in the clinical flow[112,23]. Three studies suggested that it is possible to identify language areas from rs-fMRI at the individual subject level using a template-matching procedure. One of these studies was performed in healthy children[113], and the other two in adults with brain lesions, tumours or cavernous angiomas[114,115]. Despite advances in using rs-fMRI to map language networks more studies are necessary to establish its

reliability in the setting of pediatric epilepsy, especially in young children since their distinct neurophysiology requires special considerations.

In this Chapter, we extracted language networks from rs-fMRI data in a cohort of young pediatric patients with epilepsy presenting for preoperative mapping. Rs-fMRI data was acquired while the patients were watching an animated movie. This was done retain their attention and reduce the chance for movement. Language networks were identified at the individual level by performing a spatial similarity analysis with language network templates via a template-matching procedure. Additionally, we examined lateralization concordance of these rs-fMRI-derived language networks with task-fMRI derived ones. We hypothesized that language networks can be identified from rs-fMRI by applying functional connectivity analyses, and explored methods for their visual and semi-automatic identification at the individual level.

4.2   Materials and Methods

Data was acquired clinically and analyzed retrospectively with approval from The University of Western Ontario Research Ethic Board. Children were scanned from March 2019 to December 2019, after having a short introduction on what would happen in the scanner, and the tasks they had to do. All imaging was acquired in one session. All children who underwent conventional structural imaging (T1-weighted), task- and rs-fMRI (T2-w) as part of their clinical preoperative epilepsy protocol were included.

4.2.1 MRI acquisition and experimental paradigm

Imaging was acquired on a GE 1.5 Tesla MRI scanner. Standard anatomical imaging included T1-weighted Fast Acquisition with Multiphase (FAME) in 1 x 1 x 1 mm voxels with the following parameters: slice thickness = 2 mm; repetition time (TR) = 9.2 ms; echo time (TE) = 4.2 ms; matrix size = 200×200; field-of-view (FOV) = 160 mm $\times$ 160 mm; acquisition time 4 min, 45 sec. For the task- and rest-based fMRI session a $T2*$ weighted echo planar imaging (EPI) sequence in 3 x 3 x 3 mm voxels was used with the following parameters: TR = 2.0 sec; TE = 40 ms; matrix size = 48 x 48; FOV = 200 x 200 mm; flip angle 60∘; slice thickness 3.5 mm.

Task-fMRI were all block designed tasks and included 3 tasks: one motor (i.e. hand open/close fist) and two language (verb generation, object naming). The language tasks consisted of verb generation and picture naming presented in a block-design scheme (rest, stimulus, rest, etc.): 5 blocks, 25 sec rest, 42 sec stimulus, ~5:50 min. For some cases, when the children showed signs of reduced tolerance to being in the scanner, a shorter version was used (3 blocks). Each patient received one-on-one pre-scan instructions and a trial run. The verb generation task consisted of an image of an animal or child engaged in an action followed by "is" (i.e. "The cat is …"). Auditory description was provided, as some children had not yet learned how to read or had language delays. The patient was asked to say out loud what they thought the animal/child was doing. As part of the picture naming task, the patients saw an image of an object or animal, and were asked to think about what they it was. During the rest blocks, "rest" was shown on the screen.

For the resting-state acquisition the children watched a stop-motion animated television series (~5 min). This was done to retain their attention and to reduce movement. Overall, the entire scanning session duration was approximately 1 hour.

4.2.2 MRI preprocessing and analysis

Resting-state time-series were preprocessed and analyzed using tools from the FMIRB FSL Software Library[11]. Briefly, standard preprocessing steps were performed: motion correction, skull stripping (i.e. remove non-brain tissue), spatial smoothing using Gaussian 5mm full-width at half maximum kernel, intensity normalization, high-pass 100sec. Next, we used Independent Component Analysis (ICA) through Model-Free FMRI Analysis (Multivariate Exploratory Linear Optimized Decomposition into Independent Components or MELODIC) to extract language networks from the resting-state data. This is a data-driven approach that decomposed the resting-state data into statistically independent components, each component represented by a spatial map and time-course. One or more component may represent a functional network. To bring all

---

[11] www.fmrib.ox.ac.uk/fsl

data in a common space, the resting-state and task spatial maps were linearly registered to the structural image and then non-linearly to a pediatric template in Montreal Neurological Institute[116]. Due to the variability in statistical thresholding of subject-level analyses, and lack of standardization of optimal ICA methodology, the resting-state analysis was performed at multiple thresholds from z = 2 to z = 6 in steps of 0.5, and ICA maps were generated for 20 (ICA_20), 30 (ICA_30), and 40 (ICA_40) target components and by automatic dimensionality estimation (ICA_auto). This allowed investigation of the effect of statistical thresholding and ICA order on the template-matching procedure.

To identify resting-state fMRI-derived language networks we performed a template-matching procedure. It was performed at the individual level by calculating the overlap between each multi-thresholded resting state ICA spatial maps and the functional language templates (previously described in detail[117]). The language templates included the following areas: in the left hemisphere: the angular gyrus, the superior frontal gyrus, the medial frontal gyrus, the inferior frontal gyrus, the inferior frontal gyrus pars orbitalis, the middle posterior temporal, posterior temporal, middle anterior temporal and anterior temporal regions; and in the right hemisphere: the middle anterior temporal and middle posterior temporal regions. These were combined into 6 language templates: bilateral, bilateral frontal, left, right, left frontal, right frontal, aimed at being comprehensive enough to capture various aspects of language presentation including language reorganization specific to different epilepsies. A similar template-matching was previously described in healthy children[113] and adults with brain lesions[114]. The DICE coefficient was calculated to objectively measure the voxel overlap between potential resting-state language components (r) vs the language templates (t). It varies between 0 and 1, with higher values indicating more similarity:

$$D = \frac{2\,(t \cap r)}{t + r}$$

For each of the 4 ICA groups and at the 9 thresholds, DICE coefficients were calculated to generate 36 matrices of rs-fMRI target components x language templates overlap. This visual summarization of data also allowed investigation of the effect of z-threshold and ICA order on the template-matching process.

To identify language networks, for each individual subject, rs-fMRI target components were ranked according to the highest DICE coefficient, and those with the highest overall overlap with language templates, across all thresholds and all four ICA order groups map were selected. From these, the best 3 rs-fMRI ICA components across all thresholds were further inspected as candidates for the language network. Next, percent specificity and sensitivity were calculated for each participant at the identified language components. In the listed equations, r is resting-state language components, and t is language templates.

$$\text{Specificity} = \frac{t \cap r}{r} \text{ x } 100$$

$$\text{Sensitivity} = \frac{t \cap r}{t} \text{ x } 100$$

Task-fMRI data was preprocessed using the same preprocessing steps as the rs-fMRI data. The block-design (rest, stimulus) was analyzed using standard general linear model methods: z-threshold > 2.1 and a Gaussian Field Theory corrected cluster p threshold of 0.05 as implemented in FSL's FEAT (FMRI Expert Analysis Tool). The activation maps obtained were used to confirm that the selected resting-state ICA components are related to the language network. Specifically, we used FSL's utility "fslcc" to calculate the spatial correlation, quantified as Pearson's r for each pairwise inter-voxel cross-correlation (r > .207), of the task-fMRI maps and resting-state ICA maps within the language templates. By doing this we explored if the language components identified using the template-matching procedure correspond with task-fMRI maps, thereby confirming them as part of the language network.

4.2.3 Lateralization

Lateralization was calculated using the laterality index (LI) formula:

$$LI = \frac{L - R}{L + R}$$

where L is is activated voxels in the left hemisphere within the left language mask, and R is activated voxels in the right hemisphere with the right language mask. LI ranged from -1 (completely right lateralized) to +1 (completely left lateralized). In concordance with prior studies bilateral language representation was defined in the -0.2 to 0.2 range[118].

4.3 Results

Thirteen children underwent a clinical fMRI during that period. Demographic and baseline clinical variables for the 13 patients included in the study were collected by chart review, shown in Table 4-1.

Table 4-1 Summary of demographic and clinical data for 13 cases.

Case no.	Age at fMRI (yrs), sex	Age at seizure onset (yrs)	Epileptogenic zone	Etiology
1	7, M	4	Left front or generalized	N/A
2	7, F	3	Left occipital	N/A
3	12, F	2	Left temporal	Cortical dysplasia
4	14, F	13	Left temporal-hippocampal	Left temporal ganglioglioma
5	8, M	3.5	Left frontal	N/A
6	7, F	N/A	Left occipital and temporal	Sturge Weber
7	7, F	5	Left frontal-parietal-temporal	Focal cortical dysplasia
8	13, F	10	Right frontal	Polymicrogyria
9	6, M	10 months	Temporal	N/A
10	17, F	7	Temporal	Hippocampal sclerosis
11	12, M	9	Left temporal	N/A
12	12, M	10	Left fronto-temporal	Focal cortical dysplasia
13	15, F	7.5	Fronto-temporal-parietal	Glioneuronal tumour

Average age was 10.54 ± 3.69 years (range = $6 - 17$; mode = 7), and 8 of the participants were female (62%). Most common epileptogenic zone was temporal cortex. Findings of rs-fMRI-derived language networks identification presented in Table 4-2, and the maps

are illustrated in Figure 4-1 . Some of the FOV of the MRI were restricted as the imaging were acquired clinically and did not always have the same protocol.

Table 4-2. Results of rs-fMRI language network selection. Comparison with language templates and with task-fMRI. LI, laterality index; hemi, hemisphere; verbgen, verb generation task, picname, pic naming task.

Rs-fMRI overlap with language templates						Task Lateraliza-tion
Age	Overlap	Sensitivity (%)	Specificity (%)	LI (ratio)	LI (hemi)	verbgen; picname
7	0.36	64.45	29.88	0.19	bilateral	right, right
7	0.28	44.50	30.11	0.21	left	right, right
12	0.40	36.96	45.66	-0.95	right	bilateral, right
14	0.38	51.15	51.26	-0.88	right	right
8	0.33	29.91	37.33	0.96	left	left
7	0.26	19.50	41.17	-0.84	right	right
7	0.39	47.57	34.22	0.04	bilateral	bilateral
13	0.35	48.34	37.57	0.90	left	N/A
6	0.40	47.30	35.69	-0.01	bilateral	right
17	0.27	45.27	31.44	0.06	bilateral	right
12	0.36	54.22	32.38	-0.31	right	left, left
12	0.34	34.77	45.51	0.25	left	bilateral, right
15	0.31	54.21	25.05	-0.34	right	right, right
Group	0.34 ± 0.05	44.47 ± 11.74	36.71 ± 7.47			
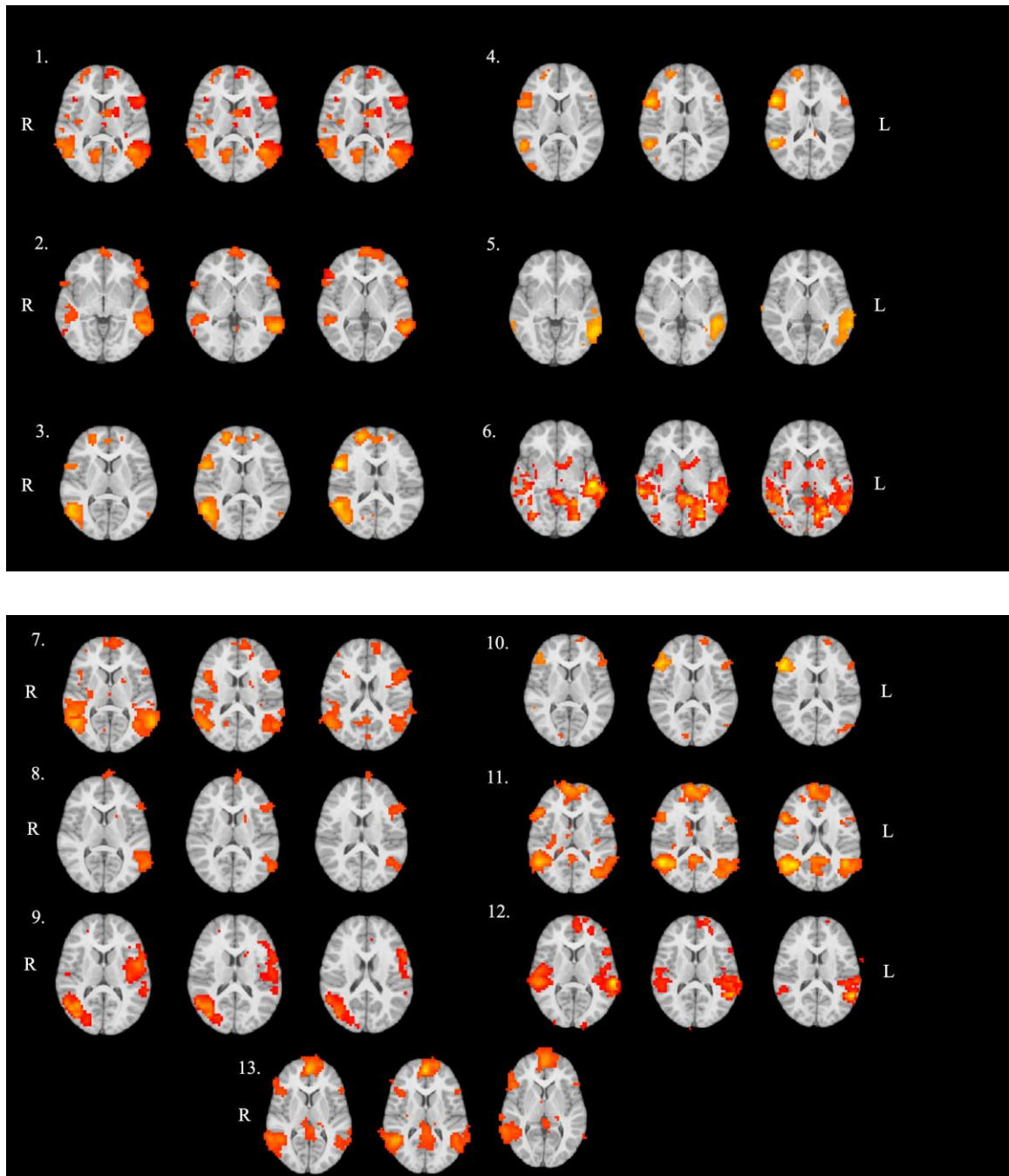
Figure 4-1 Resting-state fMRI language network maps. Cases 1 to 13; L, left. R, right. Activation maps are represented on MNI Template 3 x 3 x 3 mm.

For each subject, the language components with the highest overlap with language templates, across all thresholds and ICA groups were identified. Optimal z-threshold and ICA order (ICA_auto to ICA_40) varied substantially at the individual level. At the group level, for 92% (12/13) of subjects the ICA order at which the highest overlap was

achieved included at least 30 target components. Optimal statistical z-thresholding varied substantially with highest overlap at z = 4 or 5 for 38% of patients (5/13), see Appendix B.

Next, for each subject Maximum DICE Coefficient matrices (resting-state components that best match language templates), were generated, example seen in Figure 4-2. In some cases, the language network was fragment across several components: 7 cases had language across two components, and 1 case across 3 components
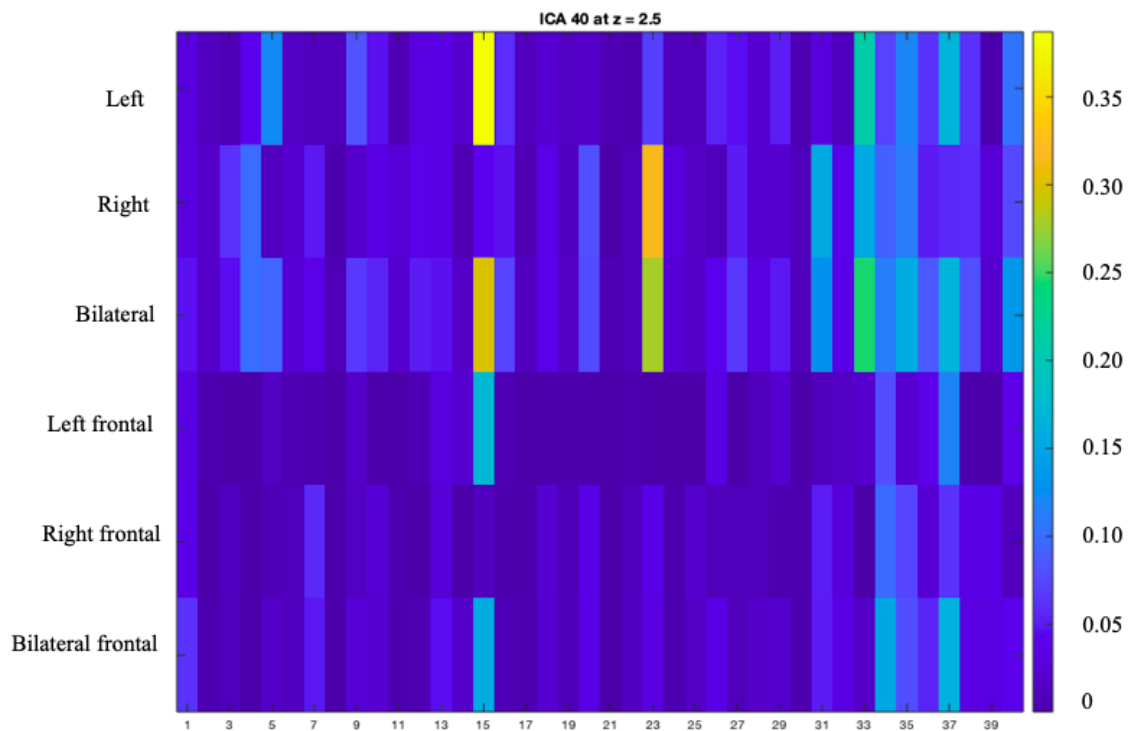
Figure 4-2. Representative subject-specific Maximum Dice Coefficient Matrix at ICA with 40 components z = 2.5. X-axis indicates the ICA component number used in the calculation. Y-axis denotes the masks used for template-matching. Colormap illustrates Dice coefficient values: yellow represents high spatial overlap, and dark blue low spatial overlap of template and ICA components. Case number 7.

Concordance between the resting-state language components and language templates was on average 0.34 ± 0.05 (range 0.26 - 0.40), with average sensitivity 44.47 ± 11.74 (range 19.50 - 64.45), and average specificity 36.71 ± 7.47 (range 25.05 - 51.26). Specificity increased while sensitivity decreased at higher z-thresholds. Verb generation task was successful in 92% of cases, while object naming in 54% of cases. Rs-fMRI was considered usable in each case.

In terms of lateralization, verb generation task-fMRI language indicated language on the left for 2 cases (17%), right for 7 cases (58%), bilateral for 3 cases (25%). In two cases, verb generation task indicated bilateral language while object naming indicated it on the right (see Table 4-2). The identified resting-state language components yielded a significant inter-voxel spatial cross-correlation with the verb generation task-fMRI spatial maps (Pearson's $r > .207$), thereby confirming good overlap between task-related activation and resting-state language networks within the language templates.

According to rs-fMRI, language was on the left for 4 cases (31%), right for 5 cases (38%), bilateral for 4 cases (31%). In 3 cases, rs-fMRI showed bilateral language while task-fMRI showed right lateralization. Some cases had partial agreement: case 3, verb generation resulted in bilateral language and picture naming in right language, while rs-fMRI showed right language; case 12, verb generation resulted in bilateral language and picture naming in right language, while rs-fMRI showed left language. In case 2, both tasks indicated right language while rs-fMRI indicated left language. Overlap between rs-fMRI language networks and task-fMRI language networks illustrated for two cases at Figure 4-3.
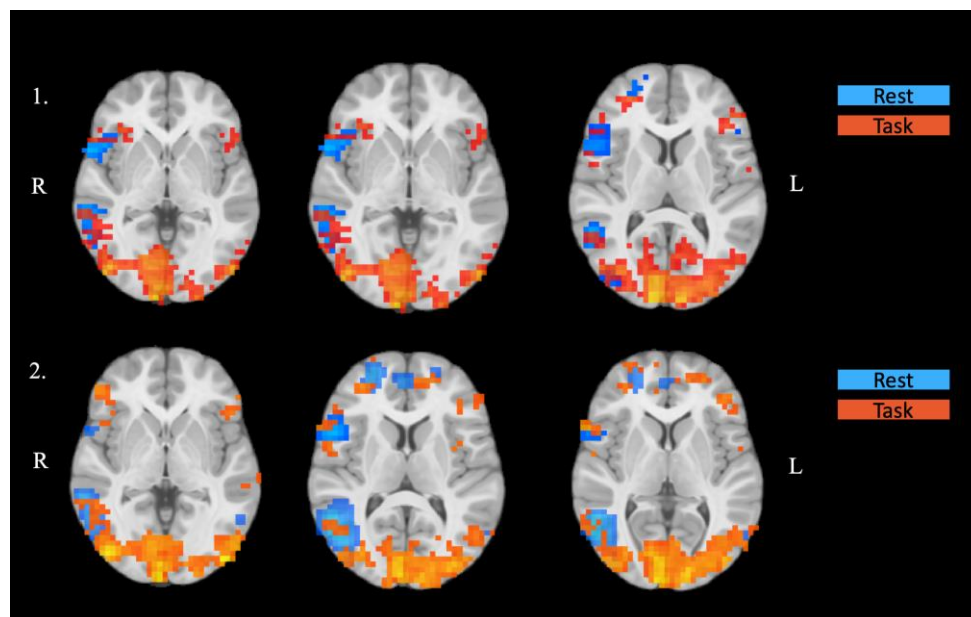
Figure 4-3. Rs-fMRI and task-fMRI language network maps for Case 4 (first row) and Case 3 (second row). Activation maps are represented on MNI Template 3 x 3 x 3 mm. L, left; R, right.

4.4   Discussion

Our study supports the growing literature that language networks can be extracted from rs-fMRI. In our sample of relatively homogenous cases of epilepsy, language networks were identified at the subject-level using a templated matching method. There was moderate to good concordance to task-fMRI.

4.4.1 Language network selection

Optimal variables for resting-state preprocessing varied significantly for each case, which was expected considering the inherent inter-individual variability characteristic of subject-level analyses. ICA dimensionality impacts the spatial topology of the resultant components, with low model order (~20) risking omission of networks and high model order (<70) leading to network fragmentation. We found that language network was best captured when ICA was performed with 30 to 50 target components. In most cases (92%) language was represented across 1 or 2 components, most commonly 2. Past studies report an increase in concordance with task-fMRI at increasing order of components[119].

As opposed to task-fMRI for which statistical thresholding is known to be relatively arbitrary and impact lateralization, data-driven ICA rs-fMRI may be more robust as it can, to some extent independently isolate sources of noise[120]. At low statistical thresholds there may be artificial overlap due to noise. We found best overlap at $z = 4$ or $z = 5$, higher than the commonly used $z = 2.3$ for task-fMRI.

Average concordance of rs-fMRI language components with language templates was DICE = 0.34 ± 0.05, slightly higher than another study using a similar template-matching procedure, DICE = 0.30 ± 0.16[113]. Average specificity $36.7 \pm 7.5\%$ and sensitivity $44.5 \pm 11.7\%$ were in agreement with previous reports [113,114]. Two earlier studies using a similar template-matching procedure reported a specificity of $36 \pm 5\%$[114], and $32.2 \pm 8.9\%$[113] when comparing rs-fMRI data with language templates, higher than task-fMRI data with language templates, $21 \pm 5\%$[114], and $30.9 \pm 12.9\%$[113]. The authors used a different method than the one used in this study to calculate sensitivity (number of activated voxels within the language templates). The calculated metrics, DICE, specificity, sensitivity, are used to classify the rs-fMRI ICA components as potentially being part of the language network. Visual inspection is still required, but the template-matching procedure allows, firstly, the visual and numeric comparison of the overlap of all components with the language templates (e.g. Figure 4-2, MaxDICE matrix), and next identification of potential language components from a reduced number of options.

There have been several attempts to categorize ICA components objectively, but there is no standardization, and visual inspection remains the most common[121,122]. We objectively selected language components by using a template-matching procedure based on well-validated language templates, similar to previous studies[113–115]. The brain regions included in the language template were chosen because they have been shown to reliably and extensively activate during multiple language tasks across healthy participants, while accounting for individual differences in anatomical variations [117]. Therefore, this method should be flexible enough to capture variable language reorganization. However, to our knowledge this is the first report of its use in a pediatric cohort with epilepsy.

Other methods for analyzing rs-fMRI for presurgical planning have been previously reviewed in detail, and include seed-based connectivity analysis, multilayer perceptron (i.e. artificial neural network), graph theory [123,124]. Comparing these methods with ICA is beyond the scope of this study but a significant advantage of ICA methodology is that it does not require *a priori* knowledge about seed placement nor a training phase for the machine learning algorithm. This is a significant consideration when assessing the developing brain.

4.4.2 Special considerations in pediatric population

Age at seizure onset and age are known factors impacting language lateralization in the setting of epilepsy. We found that rs-fMRI mapping indicated atypical language in 69% of the cases examined (range 6-17, average 10.5 years of age). This is in agreement with previous studies that reported 67.7% in a cohort of epilepsy patients using task-fMRI (range 8-18, average 13 years of age)[98]. Other studies in older children (range 13.2 – 17, average 16.3) report less atypical representation (10 – 24%)[109]. These results are not completely surprising considering that there is a known increase in lateralization of language functions to the left hemisphere with age in healthy children. In the setting of epilepsy, the increase in lateralization of language functions to the left hemisphere with age is complicated by the neural plasticity induced by epilepsy (e.g. location of the epileptogenic focus, age at seizure onset) and that characteristic of normal language development. Another factor to consider is that our relatively young and small cohort (n = 13) is not a general representation of the entire pediatric epilepsy population.

Past studies have shown that early seizure onset, before 5 years of age, is associated a higher likelihood of language reorganization and atypical lateralization (non-left)[125]. In our sample, 46% (6/13)of cases presented with age at seizure onset ≤ 5 (Table 1). Accordingly, language presentation in 5 of these cases (case 1, 2, 3, 7, 9) was either bilateral or right lateralized, suggesting that there may be language reorganization.

Our pediatric cohort had an average age of 10.5 ± 3.7, with 46% of children under 10 years of age. Both stimulation and task-fMRI based language mapping in very young

children are technically challenging. Although cortical stimulation allows the most precise mapping, it is less reliable in children younger than 10 years than in adults. Some of the factors that are recognized to contribute to unpredictable results are cortical immaturity (e.g. reduced myelination and greater production of small fibers), cortical malformations that can in turn affect afterdischarge thresholds, need for increased charge density to reach threshold for clinical response, etc. Sheovon et al (2007) reviewed the results of subdural electrode mapping in 30 younger children (4.7 – 14.9 years) and adults, and reported that children younger than 10.2 years (median 7.8 years) had significantly more negative mapping sites than older children (median 13.3) and adults.

Moreover, the limitations of task-fMRI extend beyond the requirement for compliance and task performance. Several studies suggest that the degree of language lateralization may dependent on the type of language task, with expressive tasks showing better results than receptive tasks. Verb generation is reported to lateralize language better than picture naming, and have higher concordance with stimulation techniques[126]. In our study, children seemed to prefer the verb generation task. Object naming was unsuccessful in half the cases resulting in only occipital activation. It is possible the verb generation was more engaging since it also had an auditory component. This brings into question the reliability of task-fMRI studies in young children with epilepsy. Recently, Desai et al. (2008) reported 93% correlation in lateralization when comparing task-fMRI with rs-fMRI language mapping in pediatric epilepsy (>10 years old). In our study, we had only one case (no. 2), in which task and resting-state were in complete disagreement. Rs-fMRI indicated left lateralization with a LI of 0.21, which is very close to bilateral (i.e. 0.2), while the tasks showed right lateralization. It is worth nothing that that case 2 is a 7 year old child with seizure onset at 4 years of age, and so bilateral representation would not be unusual.

Importantly, task-fMRI and rs-fMRI inherently measure different aspects of brain function. In case 1, 9, 10, rs-fMRI showed bilateral language while task-fMRI showed right lateralization. The reason for this may be that rs-fMRI covers a larger portion of the language network than that revealed by focal activation of the verb generation task.

From a neurosurgical perspective, a more comprehensive language representation can focus electrode placement and increase the yield of stimulation studies. Task-fMRI is limited in that it only indicates brain areas involved in the specific task tested. It is important to note that rs-fMRI mapping will likely indicate areas that although may be involved in language processing to varying degrees, may not be necessarily critical to function, and so may still be considered for resection. For example, rs-fMRI derived language maps may include areas related to higher cognitive aspects of language in addition to those critical for speech production. In contrast, positive stimulation sites indicates areas that produce speech arrest but miss the ones measurable only by comprehensive neurocognitive testing.

In our opinion, stimulation studies, when feasible, remain clinically necessary. Rs-fMRI can be a complementary method to obtain information for presurgical planning in situations when other clinically validated methods are not available or are unreliable. Its integration in clinical flow can broaden the patient population that can be preoperatively mapping to include young pediatric cases. Further studies should confirm rs-fMRI results with stimulation mapping and postoperative clinical outcomes in large pediatric cohorts with varying ages.

4.5   Conclusion

Rs-fMRI-derived language networks data were identified at the subject-level using a templated matching method. There was substantial inter-individual variability in optimal rs-fMRI processing variables. More than half of the cases in our study presented atypical language, emphasizing the need for mapping. There was good concordance with task-fMRI. Overall, these data suggest that this technique may be used to preoperatively identify language networks in pediatric cases. Our approach can be particularly useful in cases where the children are too young to undergo task-fMRI. While further studies are required to establish rs-fMRI language mapping, it may be used to optimize presurgical planning of electrode placement and thereby guide the surgeon's approach to the epileptogenic zone.

Chapter 5

5 Conclusions and future directions

The function and structure of the human brain develop and change across the lifespan in accordance with genetic, environmental factors and experience. They are inextricably linked to each other and to behavior. The current thesis, had as objectives to examine brain structure and function characteristics at the individual level through 1) the lens of healthy aging, 2) their visualization in a pilot augmented reality application for neurosurgical procedures, 3) and in the setting of brain mapping for pediatric epilepsy. In this current Chapter, I will provide a general discussion and conclusions of each objective and the overall thesis. Finally, I will suggest potential directions for future work.

5.1 Summary and future directions

Multimodal brain imaging is a promising approach to integrate information from distinct but complementary indicators of brain function (i.e. $BOLD_{SD}$, mean BOLD, rs-FC networks) and structure (e.g. CT, tractography) to better understand the complexity of the brain and its intra- and inter-individual variability.

5.1.1 Moderating Effect of Cortical Thickness on BOLD Signal Variability Age Related Changes

In the second Chapter of the thesis we studied structure-function relationships in the setting of aging. Specifically, we examined the impact of alternations in neuroanatomical metrics (i.e. CT, GM, CA) on age-related functional $BOLD_{SD}$ changes in a group of older adults. We modelled the interaction between these structural metrics and $BOLD_{SD}$ by treating these as physiological confounds using linear mixed models. Results show that $BOLD_{SD}$ change is confounded by change in CT. Our study highlights that CT changes should be considered when evaluating $BOLD_{SD}$ alterations in aging, and provides some insight about the potential structural substrate and physiological mechanisms underlying $BOLD_{SD.}$. One of the main strengths of our design is that it is a within-subject design rather than cross-sectional and so allows for the investigation of age-related differences (i.e. intra-individual effects of the process of aging on cortical morphology and $BOLD_{SD}$)

rather than simply age differences across groups, while also controlling for inter-individual lifestyle differences. We suggested that accounting for CT age-related changes may help "unmask" the functional value of $BOLD_{SD}$, and explain some of the inconsistency reported in the literature. Overall, this supports the thesis objective and indicates that brain structure-function relationships are an important consideration in the design and interpretation of neuroscience studies. Future studies could consider regional $BOLD_{SD}$ changes in the context of functional networks. Pursing this direction while accounting for CT and other possible confounding factors such as dopaminergic neurotransmission, socioeconomic background etc., should reveal new insights into the mechanisms behind age-related neural processes.

5.1.2 Visualization of Multimodal Brain connectivity for Neurosurgical Planning using Augmented Reality

In the third Chapter, we examined structure-function relationships at the individual level by 1) modelling brain structures, 2) calculating SC and FC connectivity, 3) visualizing them in AR in an intuitive and interactive way. Many neurosurgical procedures require preoperative identification of eloquent cortex to minimize post-operative deficit. Therefore, it is be helpful to preoperatively visualize and understand structure-function interactions when planning a surgical trajectory. Our application can allow the user to explore the patient anatomy and try different surgical approaches in a low-stakes environment. We conducted a pilot user testing experiment that indicated the application is easy and intuitive to use. With further development it could also be used a s a potential educational model for surgical trainees. Therefore, future directions include: optimizing the processing pipeline from the MRI scans to the models in AR, modelling the brain of a person with a brain tumour, and testing it on trainees and experienced surgeons. In this Chapter we demonstrated a clinical use for multimodal brain connectivity data visualization, highlighting the utility of studying structure-function relationships.

5.1.3 Presurgical brain mapping of the language network in pediatric epilepsy using resting-state fMRI

In the fourth Chapter, we studied structure-function relationships through a clinical lens. Preoperative language localization is necessary to minimize the risk of post-operative

deficits. Epilepsy is associated with significant language network reorganization, especially in the case of children, since their brains are more plastic. Therefore, structure-function relationships are more unexpected and variable. For example, often localizing language through anatomical landmarks is unreliable. We mapped language from rs-fMRI data (collected preoperatively) using a template-matching procedure. Specifically, using a data-driven analysis method (i.e. independent component analysis), we obtained multiple functional networks and classified these based on language templates. Then, we compared the identified language networks with findings from language task-fMRI. Results indicated moderate overlap, with significant inter-individual variability in language network representation. Overall, these data indicate that this approach may be used to map language in pediatric cases, especially when the children are too young to undergo task-fMRI. Future studies with larger samples and results from cortical stimulation are required to validate our rs-fMRI language mapping procedure.

5.2   Concluding remarks

The investigation brain structure-function relationships in health and illness through multimodal imaging remains a key question in neuroscience, with evolving applications in neurosurgery. Our study on CT and $BOLD_{SD}$ contributes to the growing body of knowledge on $BOLD_{SD}$, and can help inform the design of basic neuroscience studies. It emphasized the point that structure-function relationships vary across brain regions both at the individual level and between individuals. The intuitive and interactive visualization of brain connectivity measures such as SC and FC in AR can provide an educational platform for surgical trainees to learn the patient anatomy in its functional context and plan surgeries by testing different surgical trajectories. It illustrates and allows for visual exploration of whole-brain structure-function relationships. The third study on pediatric epilepsy, a disorder associated with significant cortical plasticity and functional reorganization, underscores that structure can shape function and vice versa. The novelty of this study consists of the use of an emerging rs-fMRI template-matching procedure to map language.

References

1. Broca, P. Remarques sur le siège de la faculté du langage articulé suivies d'une observation d'aphemie. *Bull Soc Anthr.* (1861).

2. Whitaker, H. A. & Selnes, O. A. Broca's area: A problem in language-brain relationships. *Linguistics* (1975). doi:10.1515/ling.1975.13.154-155.91

3. Whitaker, H. A. & Selnes, O. A. ANATOMIC VARIATIONS IN THE CORTEX: INDIVIDUAL DIFFERENCES AND THE PROBLEM OF THE LOCALIZATION OF LANGUAGE FUNCTIONS. *Ann. N. Y. Acad. Sci.* (1976). doi:10.1111/j.1749-6632.1976.tb25547.x

4. Storsve, A. B. *et al.* Differential longitudinal changes in cortical thickness, surface area and volume across the adult life span: regions of accelerating and decelerating change. *J. Neurosci.* **34**, 8488–98 (2014).

5. Penfield, W. Combined regional and general anesthesia for craniotomy and cortical exploration: Part i. Neurosurgical considerations. *Curr. Res. Anesth. Analg.* (1954). doi:10.1213/00000539-195401000-00027

6. de Ribaupierre, S., Wang, A. & Hayman-Abello, S. Language Mapping in Temporal Lobe Epilepsy in Children: Special Considerations. *Epilepsy Res. Treat.* **2012**, 1–11 (2012).

7. De Ribaupierre, S. *et al.* Presurgical language mapping in children with epilepsy: Clinical usefulness of functional magnetic resonance imaging for the planning of cortical stimulation. *Epilepsia* **53**, 67–78 (2012).

8. Bitar, R. *et al.* MR pulse sequences: What every radiologist wants to know but is afraid to ask. *Radiographics* (2006). doi:10.1148/rg.262055063

9. Evans, A. C., Collins, D. L. & Milner, B. An MRI- Based Stereotactic Atlas from 250 Young Normal Subjects. in *Society for Neuroscience Abstracts* (1992).

10. Evans, A. C. *et al.* Anatomical mapping of functional activation in stereotactic coordinate space. *Neuroimage* (1992). doi:10.1016/1053-8119(92)90006-9

11. Dale, A. M., Fischl, B. & Sereno, M. I. Cortical surface-based analysis. I. Segmentation and surface reconstruction. *Neuroimage* **9**, 179–194 (1999).

12. Fischl, B., Sereno, M. I. & Dale, A. M. Cortical surface-based analysis: II. Inflation, flattening, and a surface-based coordinate system. *NeuroImage* (1999). doi:10.1006/nimg.1998.0396

13. Evans, A. C., Janke, A. L., Collins, D. L. & Baillet, S. Brain templates and atlases. *NeuroImage* (2012). doi:10.1016/j.neuroimage.2012.01.024

14. Wandell, B. A. Clarifying Human White Matter. *Annu. Rev. Neurosci.* **39**, 103–128 (2016).

15. Soares, J. M., Marques, P., Alves, V. & Sousa, N. A hitchhiker's guide to diffusion tensor imaging. *Front. Neurosci.* (2013). doi:10.3389/fnins.2013.00031

16. Ogawa, S., Lee, T. M., Kay, A. R. & Tank, D. W. Brain magnetic resonance imaging with contrast dependent on blood oxygenation. *Proc. Natl. Acad. Sci. U. S. A.* (1990). doi:10.1073/pnas.87.24.9868

17. Kwong, K. K. *et al.* Dynamic magnetic resonance imaging of human brain activity during primary sensory stimulation. *Proc. Natl. Acad. Sci. U. S. A.* (1992). doi:10.1073/pnas.89.12.5675

18. BANDETTINI, P. A. SEVEN TOPICS IN FUNCTIONAL MAGNETIC RESONANCE IMAGING. *J. Integr. Neurosci.* (2009). doi:10.1142/s0219635209002186

19. Harris, J. J., Reynell, C. & Attwell, D. The physiology of developmental changes in BOLD functional imaging signals. *Developmental Cognitive Neuroscience* (2011). doi:10.1016/j.dcn.2011.04.001

20. Ulrich, X. & Yablonskiy, D. A. Separation of cellular and BOLD contributions to T2∗ signal relaxation. *Magn. Reson. Med.* (2016). doi:10.1002/mrm.25610

21. Ogawa, S. *et al.* Functional brain mapping by blood oxygenation level-dependent contrast magnetic resonance imaging. A comparison of signal characteristics with a biophysical model. *Biophys. J.* (1993). doi:10.1016/S0006-3495(93)81441-3

22. Sair, H. I. *et al.* Presurgical brain mapping of the language network in patients with brain tumors using resting-state fMRI: Comparison with task fMRI. *Hum. Brain Mapp.* **37**, 913–923 (2016).

23. Lee, M. H. *et al.* Clinical resting-state fMRI in the preoperative setting are we ready for prime time? *Topics in Magnetic Resonance Imaging* **25**, 11–17 (2016).

24. Biswal, B., Zerrin Yetkin, F., Haughton, V. M. & Hyde, J. S. Functional connectivity in the motor cortex of resting human brain using echo-planar mri. *Magn. Reson. Med.* (1995). doi:10.1002/mrm.1910340409

25. Smitha, K. A. *et al.* Resting state fMRI: A review on methods in resting state connectivity analysis and resting state networks. *Neuroradiology Journal* (2017). doi:10.1177/1971400917697342

26. Fox, M. D. & Raichle, M. E. Spontaneous fluctuations in brain activity observed with functional magnetic resonance imaging. *Nat. Rev. Neurosci.* (2007). doi:10.1038/nrn2201

27. Tanaka, N. & Stufflebeam, S. M. Presurgical Mapping of the Language Network Using Resting-state Functional Connectivity. *Top. Magn. Reson. imaging TMRI* **25**, 19–24 (2016).

28. Fitts, P. M. The information capacity of the human motor system in controlling the amplitude of movement. *J. Exp. Psychol.* (1954). doi:10.1037/h0055392

29. Salat, D. *et al.* Age-Associated Alterations in Cortical Gray and White Matter Signal Intensity and Gray to White Matter Contrast. *Neuroimage* **48**, 21–28 (2009).

30. Thambisetty, M. *et al.* Longitudinal changes in cortical thickness associated with normal aging. *Neuroimage* **52**, 1215–1223 (2010).

31. Hogstrom, L. J., Westlye, L. T., Walhovd, K. B. & Fjell, A. M. The structure of the cerebral cortex across adult life: Age-related patterns of surface area, thickness, and gyrification. *Cereb. Cortex* **23**, 2521–2530 (2013).

32. Jiang, J. *et al.* A longitudinal study of brain atrophy over two years in community-dwelling older individuals. *Neuroimage* (2014).

doi:10.1016/j.neuroimage.2013.08.022

33.   Panizzon, M. S. *et al.* Distinct genetic influences on cortical surface area and cortical thickness. *Cereb. Cortex* **19**, 2728–2735 (2009).

34.   Winkler, A. M. *et al.* Cortical thickness or grey matter volume? The importance of selecting the phenotype for imaging genetics studies. *Neuroimage* (2010). doi:10.1016/j.neuroimage.2009.12.028

35.   Fjell, A. M. *et al.* High consistency of regional cortical thinning in aging across multiple samples. *Cereb. Cortex* (2009). doi:10.1093/cercor/bhn232

36.   Pacheco, J., Goh, J. O., Kraut, M. A., Ferrucci, L. & Resnick, S. M. Greater cortical thinning in normal older adults predicts later cognitive impairment. *Neurobiol. Aging* **36**, 903–908 (2015).

37.   Rossini, P. M., Rossi, S., Babiloni, C. & Polich, J. Clinical neurophysiology of aging brain: From normal aging to neurodegeneration. *Progress in Neurobiology* **83**, 375–400 (2007).

38.   Fjell, A. M. *et al.* Selective increase of cortical thickness in high-performing elderly - Structural indices of optimal cognitive aging. *Neuroimage* **29**, 984–994 (2006).

39.   Ziegler, D. A. *et al.* Cognition in healthy aging is related to regional white matter integrity, but not cortical thickness. *Neurobiol. Aging* **31**, 1912–1926 (2010).

40.   Tian, P. *et al.* Cortical depth-specific microvascular dilation underlies laminar differences in blood oxygenation level-dependent functional MRI signal. *Proc. Natl. Acad. Sci.* (2010). doi:10.1073/pnas.1006735107

41.   Zhao, Y., Wen, J., Cross, A. H. & Yablonskiy, D. A. On the relationship between cellular and hemodynamic properties of the human brain cortex throughout adult lifespan. *Neuroimage* (2016). doi:10.1016/j.neuroimage.2016.03.022

42.   Garrett, D. D., Kovacevic, N., McIntosh, A. R. & Grady, C. L. Blood Oxygen Level-Dependent Signal Variability Is More than Just Noise. *J. Neurosci.* **30**, 4914–4921 (2010).

43.   Grady, C. L. & Garrett, D. D. Understanding variability in the BOLD signal and why it matters for aging. *Brain Imaging and Behavior* **8**, 274–283 (2014).

44.   Armbruster-Genc, D. J. N., Ueltzhoffer, K. & Fiebach, C. J. Brain Signal Variability Differentially Affects Cognitive Flexibility and Cognitive Stability. *J. Neurosci.* **36**, 3978–3987 (2016).

45.   Garrett, D. D., Kovacevic, N., McIntosh, A. R. & Grady, C. L. The modulation of BOLD variability between cognitive states varies by age and processing speed. *Cereb. Cortex* **23**, 684–693 (2013).

46.   Guitart-Masip, M. *et al.* BOLD Variability is Related to Dopaminergic Neurotransmission and Cognitive Aging. *Cereb. Cortex* **26**, 2074–2083 (2016).

47.   Burzynska, A. Z. *et al.* White matter integrity supports BOLD signal variability and cognitive performance in the aging human brain. *PLoS One* (2015). doi:10.1371/journal.pone.0120315

48.   Nomi, J. S., Bolt, T. S., Ezie, C. E. C., Uddin, L. Q. & Heller, A. S. Moment-to-Moment BOLD Signal Variability Reflects Regional Changes in Neural Flexibility

across the Lifespan. *J. Neurosci.* **37**, 5539–5548 (2017).

49. Kielar, A. *et al.* Identifying dysfunctional cortex: Dissociable effects of stroke and aging on resting state dynamics in MEG and fmri. *Front. Aging Neurosci.* (2016). doi:10.3389/fnagi.2016.00040

50. Scarapicchia, V., Mazerolle, E. L., Fisk, J. D., Ritchie, L. J. & Gawryluk, J. R. Resting state BOLD variability in Alzheimer's disease: A marker of cognitive decline or cerebrovascular status? *Front. Aging Neurosci.* (2018). doi:10.3389/fnagi.2018.00039

51. Zöller, D. *et al.* Disentangling resting-state BOLD variability and PCC functional connectivity in 22q11.2 deletion syndrome. *Neuroimage* (2017). doi:10.1016/j.neuroimage.2017.01.064

52. Fischl, B. & Dale, A. M. Measuring the thickness of the human cerebral cortex from magnetic resonance images. *Proc. Natl. Acad. Sci. U. S. A.* **97**, 11050–11055 (2000).

53. Salat, D. H. *et al.* Thinning of the cerebral cortex in aging. *Cereb. Cortex* **14**, 721–730 (2004).

54. Winkler, A. M. *et al.* Measuring and comparing brain cortical surface area and other areal quantities. *Neuroimage* **61**, 1428–1443 (2012).

55. Sled, J. G., Zijdenbos, A. P. & Evans, A. C. A nonparametric method for automatic correction of intensity nonuniformity in MRI data. *IEEE Trans. Med. Imaging* **17**, 87–97 (1998).

56. Reuter, M., Rosas, H. D. & Fischl, B. Highly accurate inverse consistent registration: A robust approach. *Neuroimage* (2010). doi:10.1016/j.neuroimage.2010.07.020

57. Destrieux, C., Fischl, B., Dale, A. & Halgren, E. Automatic parcellation of human cortical gyri and sulci using standard anatomical nomenclature. *Neuroimage* (2010). doi:10.1016/j.neuroimage.2010.06.010

58. Smith, S. M. *et al.* Advances in functional and structural MR image analysis and implementation as FSL. in *NeuroImage* (2004). doi:10.1016/j.neuroimage.2004.07.051

59. Jenkinson, M., Beckmann, C. F., Behrens, T. E. J., Woolrich, M. W. & Smith, S. M. FSL. *Neuroimage* (2012). doi:10.1016/j.neuroimage.2011.09.015

60. Bates, D. Fitting linear mixed models in R. *R News* (2005). doi:10.1159/000323281

61. Zuur, A. F., Leno, E. N., Walker, N. J., Saveliev, A. A. & Smith, G. M. *Mixed effects models and extensions in ecology with R. Public Health* (2011). doi:10.1016/B978-0-12-387667-6.00013-0

62. Kuznetsova, A., Brockhoff, P. B. & Christensen, R. H. B. lmerTest package: Tests in linear mixed effects models. *J. Stat. Softw.* (2017). doi:10.18637/jss.v082.i13

63. Bernal-Rusiel, J. L., Reuter, M., Greve, D. N., Fischl, B. & Sabuncu, M. R. Spatiotemporal linear mixed effects modeling for the mass-univariate analysis of longitudinal neuroimage data. *Neuroimage* (2013). doi:10.1016/j.neuroimage.2013.05.049

64. Benjamini, Y. & Yekutieli, D. The control of the false discovery rate in multiple testing under dependency. *Ann. Stat.* (2001). doi:10.1214/aos/1013699998

65. Garrett, D. D., Lindenberger, U., Hoge, R. D. & Gauthier, C. J. Age differences in brain signal variability are robust to multiple vascular controls. *Sci. Rep.* **7**, (2017).

66. Bandettini, P. A. The BOLD Plot Thickens: Sign- and Layer-Dependent Hemodynamic Changes with Activation. *Neuron* (2012). doi:10.1016/j.neuron.2012.10.026

67. Koopmans, P. J., Barth, M. & Norris, D. G. Layer-specific BOLD activation in human V1. *Hum. Brain Mapp.* (2010). doi:10.1002/hbm.20936

68. Goense, J., Merkle, H. & Logothetis, N. K. High-Resolution fMRI Reveals Laminar Differences in Neurovascular Coupling between Positive and Negative BOLD Responses. *Neuron* (2012). doi:10.1016/j.neuron.2012.09.019

69. Tang, Y., Whitman, G. T., Lopez, I. & Baloh, R. W. Brain volume changes on longitudinal magnetic resonance imaging in normal older people. *J. Neuroimaging* (2001). doi:10.1111/j.1552-6569.2001.tb00068.x

70. Shaw, M. E., Sachdev, P. S., Anstey, K. J. & Cherbuin, N. Age-related cortical thinning in cognitively healthy individuals in their 60s: The PATH Through Life study. *Neurobiol. Aging* (2016). doi:10.1016/j.neurobiolaging.2015.12.009

71. Garrett, D. D., Kovacevic, N., McIntosh, A. R. & Grady, C. L. The Importance of Being Variable. *J. Neurosci.* (2011). doi:10.1523/JNEUROSCI.5641-10.2011

72. Fagot, D. *et al. Intra-Individual Variability from a Lifespan Perspective: A Comparison of Latency and Accuracy Measures*. *Journal of Intelligence* **6**, (2018).

73. Samanez-Larkin, G. R., Kuhnen, C. M., Yoo, D. J. & Knutson, B. Variability in Nucleus Accumbens Activity Mediates Age-Related Suboptimal Financial Risk Taking. *J. Neurosci.* (2010). doi:10.1523/JNEUROSCI.4902-09.2010

74. Chan, M. Y. *et al.* Socioeconomic status moderates age-related differences in the brain's functional network organization and anatomy across the adult lifespan. *Proc. Natl. Acad. Sci. U. S. A.* (2018). doi:10.1073/pnas.1714021115

75. Abhari, K. *et al.* Training for planning tumour resection: Augmented reality and human factors. *IEEE Trans. Biomed. Eng.* **62**, 1466–1477 (2015).

76. Guha, D. *et al.* Augmented Reality in Neurosurgery: A Review of Current Concepts and Emerging Applications. *Can. J. Neurol. Sci.* **44**, 235–245 (2017).

77. Tang, S.-L., Kwoh, C.-K., Teo, M.-Y., Sing, N. W. & Ling, K.-V. Augmented realtiy systems for medical applications. *IEEE Eng. Med. Biol.* (1998).

78. Berryman, D. R. Augmented Reality: A Review. *Medical Reference Services Quarterly* (2012). doi:10.1080/02763869.2012.670604

79. Harders, M., Bianchi, G. & Knoerlein, B. Multimodal Augmented Reality in Medicine. in *Universal Access in Human-Computer Interaction. Ambient Interaction* (2007). doi:10.1007/978-3-540-73281-5_70

80. Rankin, T. M., Slepian, M. J. & Armstrong, D. G. Augmented Reality in Surgery. in *Technological Advances in Surgery, Trauma and Critical Care* (2015). doi:10.1007/978-1-4939-2671-8_6

81. Chicchi Giglioli, I. A., Pallavicini, F., Pedroli, E., Serino, S. & Riva, G.

Augmented Reality: A Brand New Challenge for the Assessment and Treatment of Psychological Disorders. *Computational and Mathematical Methods in Medicine* (2015). doi:10.1155/2015/862942

82.   Meola, A. *et al.* Augmented reality in neurosurgery: a systematic review. *Neurosurgical Review* (2017). doi:10.1007/s10143-016-0732-9

83.   Alaraj, A. *et al.* Role of cranial and spinal virtual and augmented reality simulation using immersive touch modules in neurosurgical training. *Neurosurgery* (2013). doi:10.1227/NEU.0b013e3182753093

84.   Luciano, C., Banerjee, P., Florea, L. & Dawe, G. Design of the ImmersiveTouchTM: a High-Performance Haptic Augmented Virtual Reality System. in *Proceedings from International Conference on Human-Computer (HCI)* (2005).

85.   Incekara, F., Smits, M., Dirven, C. & Vincent, A. Clinical Feasibility of a Wearable Mixed-Reality Device in Neurosurgery. *World Neurosurg.* (2018). doi:10.1016/j.wneu.2018.06.208

86.   Kramers, M. *et al.* Evaluation of a mobile augmented reality application for image guidance of neurosurgical interventions. *Stud. Health Technol. Inform.* (2014).

87.   Wright, T., de Ribaupierre, S. & Eagleson, R. Design and evaluation of an augmented reality simulator using leap motion. *Healthc. Technol. Lett.* (2017). doi:10.1049/htl.2017.0070

88.   Pelargos, P. E. *et al.* Utilizing virtual and augmented reality for educational and clinical enhancements in neurosurgery. *Journal of Clinical Neuroscience* (2017). doi:10.1016/j.jocn.2016.09.002

89.   Shang, H. B. pd., Zhao, W. G. & Zhang, W. F. Preoperative assessment using multimodal functional magnetic resonance imaging techniques in patients with brain gliomas. *Turk. Neurosurg.* (2012). doi:10.5137/1019-5149.JTN.5332-11.1

90.   Bakhshmand, S. M., Eagleson, R. & de Ribaupierre, S. Multimodal connectivity based eloquence score computation and visualisation for computer-aided neurosurgical path planning. *Healthc. Technol. Lett.* **4**, 152–156 (2017).

91.   Bakhshmand, S. M., Khan, A. R., de Ribaupierre, S. & Eagleson, R. MultiXplore: Visual exploration platform for multimodal neuroimaging data. *J. Neurosci. Methods* (2017). doi:10.1016/j.jneumeth.2017.07.006

92.   Ségonne, F. *et al.* A hybrid approach to the skull stripping problem in MRI. *Neuroimage* (2004). doi:10.1016/j.neuroimage.2004.03.032

93.   Dale, A. M. & Sereno, M. I. Improved Localizadon of Cortical Activity by Combining EEG and MEG with MRI Cortical Surface Reconstruction: A Linear Approach. *J. Cogn. Neurosci.* **5**, 162–176 (1993).

94.   Desikan, R. S. *et al.* An automated labeling system for subdividing the human cerebral cortex on MRI scans into gyral based regions of interest. *Neuroimage* (2006). doi:10.1016/j.neuroimage.2006.01.021

95.   Cross, J. H. *et al.* Epilepsy surgery in children: Time is critical. *Pediatr. Epilepsy Surg.* (2014).

96.   Jayalakshmi, S., Panigrahi, M., Nanda, S. K. & Vadapalli, R. Surgery for

childhood epilepsy. *Ann. Indian Acad. Neurol.* (2014). doi:10.4103/0972-2327.128665

97. Holland, S. K. *et al.* Functional MRI of language lateralization during development in children. *International Journal of Audiology* (2007). doi:10.1080/14992020701448994

98. Yuan, W. *et al.* fMRI shows atypical language lateralization in pediatric epilepsy patients. *Epilepsia* (2006). doi:10.1111/j.1528-1167.2006.00474.x

99. Sepeta, L. N. *et al.* Reduced language connectivity in pediatric epilepsy. *Epilepsia* (2015). doi:10.1111/epi.12859

100. Önal, Ç. *et al.* Complications of invasive subdural grid monitoring in children with epilepsy. *J. Neurosurg.* (2003). doi:10.3171/jns.2003.98.5.1017

101. Johnston, J. M. *et al.* Complications of invasive subdural electrode monitoring at St. Louis Children's Hospital, 1994-2005. *J. Neurosurg.* (2006). doi:10.3171/ped.2006.105.5.343

102. Roland, J. L. & Smyth, M. D. Recent advances in the neurosurgical treatment of pediatric epilepsy. *J. Neurosurg. Pediatr.* **23**, 411–421 (2019).

103. Austermuehle, A. *et al.* Language functional MRI and direct cortical stimulation in epilepsy preoperative planning. *Ann. Neurol.* (2017). doi:10.1002/ana.24899

104. Giussani, C. *et al.* Is preoperative functional magnetic resonance imaging reliable for language areas mapping in brain tumor surgery? Review of language functional magnetic resonance imaging and direct cortical stimulation correlation studies. *Neurosurgery* **66**, 113–120 (2010).

105. Smith, S. M. *et al.* Correspondence of the brain's functional architecture during activation and rest. *Proc. Natl. Acad. Sci. U. S. A.* (2009). doi:10.1073/pnas.0905267106

106. Rosazza, C. *et al.* Preoperative mapping of the sensorimotor cortex: Comparative assessment of task-based and resting-state fMRI. *PLoS One* (2014). doi:10.1371/journal.pone.0098860

107. Zhang, D. *et al.* Preoperative sensorimotor mapping in brain tumor patients using spontaneous fluctuations in neuronal activity imaged with functional magnetic resonance imaging: Initial experience. *Neurosurgery* (2009). doi:10.1227/01.NEU.0000350868.95634.CA

108. Roland, J. L. *et al.* A comparison of resting state functional magnetic resonance imaging to invasive electrocortical stimulation for sensorimotor mapping in pediatric patients. *NeuroImage Clin.* **23**, 101850 (2019).

109. Desai, V. R. *et al.* Language lateralization with resting-state and task-based functional MRI in pediatric epilepsy. *J. Neurosurg. Pediatr.* **23**, 171–177 (2019).

110. Roland, J. L. *et al.* Resting-state functional magnetic resonance imaging for surgical planning in pediatric patients: a preliminary experience. *J. Neurosurg. Pediatr.* (2017). doi:10.3171/2017.6.PEDS1711

111. Vadivelu, S., Wolf, V. L., Bollo, R. J., Wilfong, A. & Curry, D. J. Resting-state functional MRI in pediatric epilepsy surgery. *Pediatric Neurosurgery* (2014). doi:10.1159/000363605

112. Leuthardt, E. C. *et al.* Integration of resting state functional MRI into clinical practice - A large single institution experience. *PLoS One* **13**, 1–16 (2018).

113. Tie, Y. *et al.* Defining language networks from resting-state fMRI for surgical planning- A feasibility study. *Hum. Brain Mapp.* **35**, 1018–1030 (2014).

114. Branco, P. *et al.* Resting-State Functional Magnetic Resonance Imaging for Language Preoperative Planning. *Front. Hum. Neurosci.* **10**, (2016).

115. Zacà, D. *et al.* ReStNeuMap: A tool for automatic extraction of resting-state functional MRI networks in neurosurgical practice. *J. Neurosurg.* (2019). doi:10.3171/2018.4.JNS18474

116. Fonov, V., Evans, A., McKinstry, R., Almli, C. & Collins, D. Unbiased nonlinear average age-appropriate brain templates from birth to adulthood. *Neuroimage* (2009). doi:10.1016/s1053-8119(09)70884-5

117. Fedorenko, E., Hsieh, P. J., Nieto-Castañón, A., Whitfield-Gabrieli, S. & Kanwisher, N. New method for fMRI investigations of language: Defining ROIs functionally in individual subjects. *J. Neurophysiol.* **104**, 1177–1194 (2010).

118. Springer, J. A. *et al.* Language dominance in neurologically normal and epilepsy subjects. A functional MRI study. *Brain* (1999). doi:10.1093/brain/122.11.2033

119. Yahyavi-Firouz-Abadi, N. *et al.* Presurgical brain mapping of the ventral somatomotor network in patients with brain tumors using resting-state fMRI. *Am. J. Neuroradiol.* **38**, 1006–1012 (2017).

120. Ruff, I. M. *et al.* Assessment of the language laterality index in patients with brain tumor using functional MR imaging: Effects of thresholding, task selection, and prior surgery. *Am. J. Neuroradiol.* (2008). doi:10.3174/ajnr.A0841

121. Sui, J., Adali, T., Pearlson, G. D. & Calhoun, V. D. An ICA-based method for the identification of optimal FMRI features and components using combined group-discriminative techniques. *Neuroimage* (2009). doi:10.1016/j.neuroimage.2009.01.026

122. Kelly, R. E. *et al.* Visual inspection of independent components: Defining a procedure for artifact removal from fMRI data. *J. Neurosci. Methods* (2010). doi:10.1016/j.jneumeth.2010.03.028

123. Mitchell, T. J. *et al.* A novel data-driven approach to preoperative mapping of functional cortex using resting-state functional magnetic resonance imaging. *Neurosurgery* **73**, 969–983 (2013).

124. Hart, M. G., Price, S. J. & Suckling, J. Functional connectivity networks for preoperative brain mapping in neurosurgery. *J. Neurosurg.* **126**, 1941–1950 (2017).

125. Saltzman, J., Smith, M. Lou & Scott, K. The impact of age at seizure onset on the likelihood of atypical language representation in children with intractable epilepsy. in *Brain and Cognition* (2002). doi:10.1006/brcg.2001.1409

126. Benson, R. R. *et al.* Language dominance determined by whole brain functional MRI in patients with brain lesions. *Neurology* (1999). doi:10.1212/wnl.52.4.798

Appendices

Appendix A: Results of subjects' trials on pointing task. For each pointing task/fiber target, the average and standard deviation of the performance of all subjects (n =10) at that task was calculated. The volume and index of difficulty were constant across subjects.

	Avg	SD	Avg	SD		
Task no.	MT (seconds)		IP (u²bits/seconds)		Volume (u³)	ID (u²bits)
1	3.397	± 1.302	1.698	± 0.521	0.009224	5.198
2	7.787	± 3.745	1.653	± 1.257	0.000541	9.301
3	5.233	± 5.047	3.155	± 1.524	0.000199	10.777
4	3.318	± 1.601	3.316	± 1.247	0.000501	9.448
5	9.451	± 8.205	2.324	± 2.120	0.000128	11.403
6	11.321	± 9.220	1.301	± 0.876	0.000694	8.970
7	5.258	± 2.799	1.492	± 0.679	0.004168	6.310
8	5.340	± 3.336	2.629	± 1.862	0.000541	9.256
9	3.013	± 1.606	2.131	± 0.971	0.010089	5.103
10	6.522	± 10.968	3.438	± 2.720	0.00391	6.489
11	4.940	± 4.423	1.995	± 1.484	0.009264	5.233
12	7.970	± 6.953	1.921	± 1.606	0.00114	8.249
13	5.455	± 3.395	2.609	± 1.341	0.000201	10.703
14	11.360	± 9.287	1.705	± 1.151	5.77E-05	12.494
15	6.649	± 9.244	3.920	± 2.637	6.06E-05	12.464

16	4.333	± 3.582	5.022	± 2.855	2.45E-05	13.827
17	2.230	± 1.386	5.145	± 1.992	0.000547	9.306
18	4.302	± 2.223	2.666	± 1.904	0.000968	8.519
19	4.503	± 4.692	2.730	± 1.496	0.002858	6.965
20	4.771	± 3.030	4.500	± 3.099	2.04E-05	14.081
21	4.108	± 2.273	4.048	± 1.787	3.45E-05	13.298
22	7.562	± 5.814	1.984	± 1.208	0.000425	9.620
23	5.322	± 3.536	3.008	± 1.710	0.0001	11.723
24	6.234	± 4.895	3.070	± 1.988	0.000117	11.457

Appendix B Optimal variables for resting-state analysis

Case no.	ICA order	Z-thresh.
1	Auto 43	2.5
2	Auto 53	4
3	30	5
4	30	4
5	30	3.5
6	20	3
7	40	2.5
8	Auto 44	3
9	Auto 45	4
10	40	4
11	30	2
12	Auto 72	2
13	30	2

Curriculum Vitae

Name:	Daiana R. Pur
Post-secondary Education and Degrees:	The University of Western Ontario London, Ontario, Canada 2014 - 2018 B.MSc
	The University of Western Ontario London, Ontario, Canada 2018 - 2020 M.ESc
Honours and Awards:	Scholar's Electives 2014 - 2018
	Mitacs Globalink Research Award June - September 2019
	Western Graduate Research Scholarship 2018 - 2020
Related Work Experience:	Research Assistant Clinical Neurological Sciences The University of Western Ontario 2016 - 2018

Publications:

Journal Publications:

Pur, D.R., Kikinov, D., de Ribaupierre, S., Eagleson, R., (2019). Visualization of multimodal brain connectivity for neurosurgical planning using handheld device augmented reality. *Proceedings of the 5th World Congress on Electrical Engineering and Computer Systems and Sciences (EECSS'19), No. ICBES 126.* doi:10.11159/icbes19.126

Pur, D.R., Eagleson, R., de Ribaupierre, S. (2019). Moderating Effect of Cortical Thickness on BOLD signal variability Age-related changes. *Frontiers in Neuroscience Aging*, 11, 46. doi:10.3389/fnagi.2019.00046

Conference Publications:

Kikinov, D., **Pur, D.R.,** Eagleson, R., de Ribaupierre, S. (2020). Augmented reality visualization of MRI-guided presurgical planning. 34th International Congress on Computer Assisted Radiolog and Surgery.

Pur, D.R., Preti, M.G., Mella, N., de Ribaupierre, A., Van De Ville, D., Eagleson, R., de Ribaupierre, S. (2020). Influence of structure-function age-related changes on behavior using multimodal MR: A longitudinal study. *Alpine Brain Imaging Meeting*. Geneva, Switzerland.

Pur, D.R., Gainham, G., Mella, N., de Ribaupierre, A., Eagleson, R., de Ribaupierre, S. (2019). Task based fMRI and resting state fMRI sequences differentially modulate BOLD signal variability. *25rd Annual Meeting of the Organization for Human Brain Mapping*. Rome, Italy

Pur, D.R., Eableson R., de Ribaupierre S. (2019) Can we use resting-state fMRI to presurgically map language networks in pediatrics? Clinical Neurological Sciences Research Day, London, Canada.

Pur, D.R., Eagleson, R., de Ribaupierre, S. (2019). Interactive user interface for exploring BOLD signal variability-derived functional connectivity. *13th Annual Canadian Neuroscience Meeting,* Toronto, Canada

Pur, D.R., de Ribaupierre, S., Eagleson, R., Ansermet, E. (2018). Default Mode Network and Dorsal Attention Network anti-correlation predicts BOLD signal variability in left intraparietal sulcus and left middle frontal gyrus in older adults. *Sixth Biennial Conference on Resting State and Brain Connectivity*, Montreal, Canada

Pur, D.R., Eagleson, R., Mella, N., de Ribaupierre, A., de Ribaupierre S. (2018). The influence of cortical morphology on BOLD signal variability. *12th Annual Canadian Neuroscience Meeting,* Vancouver, Canada.

De Ribaupierre, S., **Pur, D.R**., Bakhsmand, S., Mella, N., & de Ribaupierre, A. (2017). Visualization of functional and structural connectivity in lifespan. *3rd International Conference on Basic and Clinical Multimodal Imaging.* Bern, Switzerland.